Bio-Design and Manufacturing (2021) 4:568–595
https://doi.org/10.1007/s42242-020-00120-5

REVIEW

Engineering biomimetic intestinal topological features in 3D tissue models: retrospects and prospects

Tarun Agarwal[1] · Valentina Onesto[2] · Lallepak Lamboni[3,4] · Aafreen Ansari[5] · Tapas K. Maiti[1] · Pooyan Makvandi[6] · Massoud Vosough[7,8] · Guang Yang[3]

Received: 17 October 2020 / Accepted: 15 December 2020 / Published online: 3 February 2021

Abstract

Conventional 2D intestinal models cannot precisely recapitulate biomimetic features in vitro and thus are unsuitable for various pharmacokinetic applications, development of disease models, and understanding the host-microbiome interactions. Thus, recently, efforts have been directed toward recreating in vitro models with intestine-associated unique 3D crypt-villus (for small intestine) or crypt-lumen (for large intestine) architectures. This review comprehensively delineates the current advancements in this research area in terms of the different microfabrication technologies (photolithography, laser ablation, and 3D bioprinting) employed and the physiological relevance of the obtained models in mimicking the features of native intestinal tissue. A major thrust of the manuscript is also on highlighting the dynamic interplay between intestinal cells (both the stem cells and differentiated ones) and different biophysical, biochemical, and mechanobiological cues along with interaction with other cell types and intestinal microbiome, providing goals for the future developments in this sphere. The article also manifests an outlook toward the application of induced pluripotent stem cells in the context of intestinal tissue models. On a concluding note, challenges and prospects for clinical translation of 3D patterned intestinal tissue models have been discussed.

Keywords Intestine tissue models · Microfabrication · Biophysicochemical and biomechanical cues · Coculture · Induced pluripotent stem cells

Abbreviations

2D	Two-dimensional
3D	Three-dimensional
SI	Small intestine
LI	Large intestine
CBC	Crypt base columnar cells
TA	Transit-amplifying
M cell	Microfold cell
UV	Ultraviolet
PDMS	Polydimethylsiloxane

Valentina Onesto and Lallepak Lamboni are equal contribution to this work.

✉ Tapas K. Maiti
tkmaiti@bt.iitkgp.ac.in; maititapask@gmail.com

[1] Department of Biotechnology, Indian Institute of Technology Kharagpur, Kharagpur, West Bengal 721302, India

[2] Center for Advanced Biomaterials for Health Care, Istituto Italiano di Tecnologia (IIT@CRIB), 80125 Naples, Italy

[3] National Engineering Research Center for Nano-Medicine, Department of Biomedical Engineering, College of Life Science and Technology, Huazhong University of Science and Technology, 1037 Luoyu Road, Wuhan 430074, People's Republic of China

[4] Laboratoire de Biologie Moléculaire, Institut National d'Hygiène-Togo, 26 Rue Nangbéto, Quartier Administratif-PO. Box 1396, Lomé, Togo

[5] Department of Biotechnology and Medical Engineering, National Institute of Technology Rourkela, Rourkela, Orissa 769008, India

[6] Institute for Polymers, Composites and Biomaterials (IPCB), National Research Council (CNR), Naples, Italy

[7] Department of Stem Cells and Developmental Biology, Cell Science Research Center, Royan Institute for Stem Cell Biology and Technology, ACECR, Tehran, Iran

[8] Department of Regenerative Medicine, Cell Science Research Centre, Royan Institute for Stem Cell Biology and Technology, ACECR, Tehran, Iran

PTFE	Polytetrafluoroethylene
PEG	Poly(ethylene glycol)
AA	Acrylic acid
ECM	Extracellular matrix
UV-LIGA	Ultraviolet-lithography, electroplating, and molding
PLA	Poly(lactic acid)
CVD	Chemical vapor deposition
PMMA	Poly(methyl methacrylate)
PLGA	Poly(lactic-co-glycolic acid)
PEVA	Poly-ethylene-co-vinyl-acetate
CAD	Computer-aided design
PEGDA	Poly(ethylene glycol) diacrylate
VMEPS	Vertically moving extrusion-based printing system
HUVECs	Human umbilical vein endothelial cells
TEER	Transepithelial electrical resistance
MUC17	Mucin 17
RT-PCR	Reverse transcription polymerase chain reaction
FITC	Fluorescein isothiocyanate
PCL	Poly-ε-caprolactone
ZO-1	Zonula occludens-1
P-gp	P-Glycoprotein
ALP	Alkaline phosphatase
CYP3A4	Cytochrome P450 3A4
EdU	5-Ethynyl-2′-deoxyuridine
Olfm4	Olfactomedin 4
CK20	Keratin 20
MUC2	Mucin 2
E-cad	E-cadherin
ISC	Intestinal stem cell
RGD	Arginine-glycine-aspartate
GAGs	Glycosaminoglycans
Wnt	Wingless-related integration site
TGF-β	Transforming growth factor beta
FGF	Fibroblast growth factors
LGR5	Leucine-rich repeat-containing G-protein coupled receptor 5
IFN-γ	Interferon gamma
TNF-α	Tumor necrosis factor alpha
YAP	Yes-associated protein 1
BCRP	Breast cancer resistance protein
MRP2	Multidrug resistance protein 2
iPSCs	Induced pluripotent stem cells
STAT1	Signal transducer and activator of transcription 1
ENS	Enteric nervous system
MIP-2	Macrophage inflammatory protein 2
IL-10	Interleukin 10
ISEMFs	Intestinal subepithelial myofibroblasts
SCFAs	Short-chain fatty acids
ELCs	Enterocytes-like cells
DELCs	Definite endodermal-like cells
IPLCs	Intestinal progenitor-like cells
HLCs	Hindgut-like cells
EGF	Epidermal growth factor
5-aza	5-Aza-2′-deoxycytidine
BIO	6-Bromoindirubin-3′-oxime
DAPT	N-[(3,5-difluorophenyl)acetyl]-L-alanyl-2-phenyl-1,1-dimethylethyl ester-glycine
WRN	Wnt3A,R-spondin,Noggin
PEPT1	Peptide transporter 1
SIOs	Small intestinal organoids
Cos	Colonic organoids
BMPs	Bone morphogenetic proteins
SATB2	Special AT-rich sequence-binding protein 2
HOX	Homeobox
WDR43	WD Repeat Domain 43
TALEN	Transcription activator-like effector nuclease
CFTR	Cystic fibrosis transmembrane conductance regulator
IBD	Inflammatory bowel disease

Introduction

The intestine is one of the most vital metabolic organs involved in digestion and absorption of nutrients [1–3]. Its unique microarchitecture accompanied by the peristaltic contractions provides a much required large surface area to aid nutrient absorption [2–4]. Owing to its constant contact with gut microbiome and xenobiotics components, it is at high risk of various pathological disorders [5–7]. Thus, to find a potential treatment for these disorders, a clear understanding of their mechanistic aspects is necessary.

Animal models are still the gold standard clinical models to study intestinal anatomy, physiology, pathologies and xenobiotic-mediated tissue responses [8, 9]. However, the underlying differences with the human intestinal anatomy, gut microbiota, immunological activities, expense of animal maintenance, and ethical considerations, further limit their usage [8, 10]. Therefore, the current thrust of the healthcare and diagnostic sector is on the development of functional in vitro intestinal tissue models.

Up to date, various intestinal models, including 2D/3D or dynamic microfluidic chip-based, have been proposed and developed [1, 11]. However, limited physiological relevance of these models, in terms of topological and microenvironmental features, makes them far from actually recapitulating the complexity of the native intestinal tissue, and thus, are unsuitable for clinical applications [1, 11–14].

In this regard, decellularized intestinal submucosal tissue holds the most promising prospects as it retains, to an extent, native-like architectural and matrix's biochemical characteristics [15, 16]. Owing to these aspects, decellularized

scaffolds have generated a great wave of enthusiasm, mainly in the domain of regenerative medicines and in vitro model development [17, 18]. But their applicability is often limited by a low tissue availability, tedious non-standardized decellularization procedure, damage to the native ECM (microstructural, biochemical, and mechanical), difficult handling, and low experimental reproducibility [15, 17, 18].

Consequently, a current focus of research fraternity is on devising strategies for patterning intestine-like topologies on 2D substrates. These patterned substrates could be employed for developing biomimetic in vitro 3D tissue models. Advanced microfabrication techniques, including soft lithography, laser-induced ablation, and 3D (bio) printing, have paved the way for the same [1, 11]. In fact, cells cultured on these models exhibit more differentiated phenotype, compared to those on other conventional models [19–22]. To the best of our knowledge, to date, there exists no review that critically highlights the patterned 3D intestinal tissue models, their corresponding fabrication technologies, as well as the impact of these topological cues on cellular activity. Thus, in the present work, we have taken the opportunity to discuss these topics comprehensively. Further, we discuss the importance of various biophysical and biochemical aspects of the matrix, external biomechanical cues, and coculture strategies (with other cell types and intestinal microflora), supported by recent development in the domain. Besides, to further extend the scope of the review, aspects of stem cell engineering are also included.

Intestinal epithelium: understanding the biology of crypt-villus architecture

The intestinal epithelium is the innermost lining of the intestine, acting as a physical barrier between the internal tissue and the luminal environment and is responsible for the digestion of the chyme and absorption of the nutrients [5, 23]. The intestinal epithelium is organized into a specialized crypt/villus configuration [3, 24]. Notably, this configuration varies along the length of intestine, from the small intestine (SI) to large intestine (LI).

In the SI, the configuration consists of a villus (finger-like projection of the intestinal wall), surrounded by multiple crypts (invaginations into the intestinal wall, appropriately termed as the crypt of Lieberkuhn) [3, 24]. The villus is the site of intestinal brush-border enzyme-mediated digestion (mainly in the duodenum) and nutrient uptake (in the jejunum and ileum) [3]. The absorbed nutrients are further channelized into the blood mainstream via the underlying blood and lymphatic capillaries. The duodenum zone of SI has the longest villi (> 1 mm length) [24]. On the other hand, the crypt primarily acts as glands that secrete antimicrobial agents and several hormones. They are also characterized by the presence of an intestinal stem cell (ISC) niche [1]. In contrast, the LI does not have villi-like structures but abounds of cryptic invaginations [1].

The ISC niche is highly dynamic and is responsible for restoring the intestinal epithelium every 4–5 days [25]. It contains active multipotent ISCs (also known as crypt base columnar cells or CBCs), placed alternatively to Paneth cells [24, 26]. Besides, the stem cell niche also has a quiescent stem cell population that plays a crucial role in regenerating the ISC niche in case of any tissue injury [24]. The CBCs undergo constant proliferation and also give rise to transit-amplifying (TA) cells, which further differentiate into secretory (Paneth, goblet, enteroendocrine and tuft cell) and absorptive (enterocytes and M cell) lineages [1, 24, 26]. In contrast, LI does not have Paneth cells, and the ratio of goblet cell to enterocytes is relatively higher than in SI [1].

During the proliferation and differentiation process, the fully mature epithelial cells show a gross upward movement along the crypt-villus axis in the SI and toward the luminal surface in the LI [1]. Besides this, the damaged or apoptotic cells shred off into the intestinal lumen. Notably, unlike other differentiated epithelial cells, Paneth cells move downwards to form the part of stem cell niche [24].

The distribution and specific functions of the different cell types are illustrated in Fig. 1 and Table 1.

Developing crypt-villus architecture: the current state of the art

Over the last decade, enormous efforts have been dedicated to recapitulating the crypt-villus architecture associated with the intestinal tissue in vitro [1, 11]. This section delineates different fabrication strategies employed for developing these topological features and the impact of these topological features on the behavior of cultured intestinal cells.

Fabrication strategies

Replica molding

Replica molding is a strategy that involves the development of master mold containing patterns, followed by multiple imprinting and remolding steps to fabricate scaffolds with biomimetic 3D intestinal topology.

Photolithography has widely been employed in various fields to obtain micropatterns. Typically, it is based on the crosslinking of a photosensitive polymer or photoresist, that is selectively exposed to ultraviolet (UV) light through a photomask with a desired pattern [44]. Conventional photolithography with SU-8 photoresist on silicon wafer followed by PDMS replica molding was employed to fabricate molds for 3D villi-like hydrogel units and the PDMS fluidic

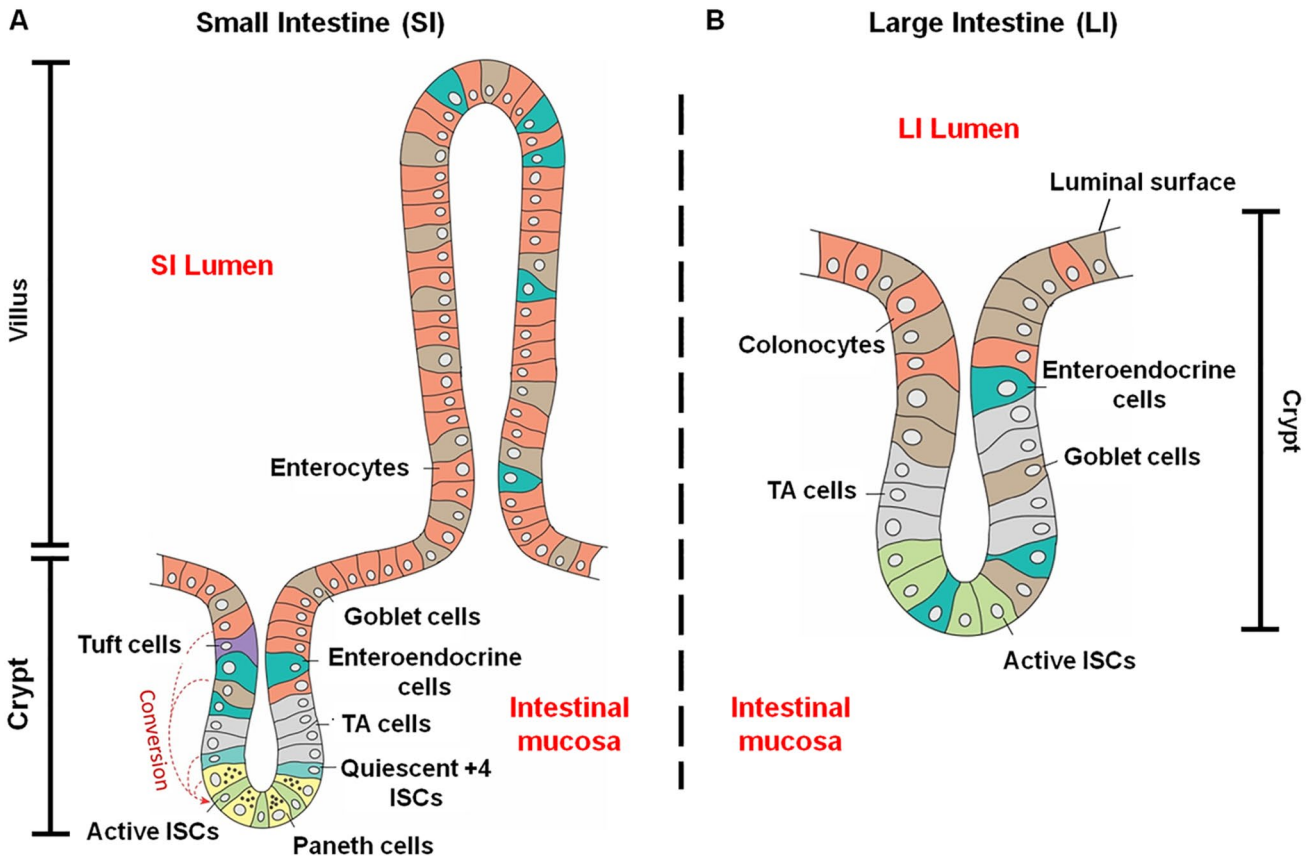

Fig. 1 Distribution of cells across the **a** crypt-villus axis of SI and **b** crypts of LI. ISC niche consisting of actively dividing ISCs (green) and Quiescent+4 ISCs (light blue) is present at the cryptic base. TA cells (gray) further differentiated to form enterocytes (in SI)/colonocytes (in LI) (orange), goblet (brown), tuft (purple), enteroendocrine (blue), and Paneth cells (yellow). Paneth cells are particularly present in the crypts of SI. Red arrow designates the ability of different cell types to convert into active ISCs. Reprinted with permission from [26]

channel [45]. The resultant alginate/collagen hydrogel units with different aspect ratios were assembled inside the fluidic channel, recreating 3D intestinal environment on-chip for culturing cells under flow conditions. In another study, the sole crypt structures in a collagen scaffold were reproduced with one-layer photolithography, within a modified Transwell (Fig. 2b) [46] or within a customized platform in which a photo-patterned hydrophilic polytetrafluoroethylene (PTFE) membrane [47]. In an effort to recreate human SI epithelium with crypts and villi, two-layer photolithography was used. The strategy involved reproducing the negative of the villi first, and then the negative of the crypts in a single mold. Two steps of polydimethylsiloxane (PDMS) soft lithography followed the preparation of micromolds; after that, crosslinked collagen hydrogel scaffolds (via EDC/NHS chemistry) were developed, reproducing crypts and villi (Fig. 2a) [48].

Recently, reaction–diffusion mediated photolithography (which involves controlled oxygen gradients within the polymerization set up) has been developed as a simple, single-step and mold-free procedure to mimic the 3D villus-like geometry using a polymeric formulation containing poly(ethylene glycol) diacrylate (PEGDA), acrylic acid (AA), and Irgacure D-2959 [49]. The dimensions and geometries of the microstructures were established by playing with fabrication parameters such as the oxygen diffusion/depletion timescales, the exposure dose, and distance to the light source. AA allowed covalent conjugation of ECM proteins (laminin or collagen), whose density could be tuned without affecting the mechanical properties of the hydrogel, making the constructs suitable for cell culture. Inexpensive and rapidly implementable UV-LIGA (lithography, electroplating, and molding) fabrication technology, involving backside exposure-based photolithography with SU-8, was used to produce an array of microneedles, with projective structure and size comparable to those of the mouse duodenal villi [50]. These molds were replicated to develop poly(lactic acid) (PLA)-based 3D scaffolds.

Table 1 Cells of intestinal tissue: distribution, major functions, and key cell markers

Cells	Localization	Major functions	Key cell markers	References
CBC cells	Crypt	Multipotent active ISC population. Bulk of proliferation and maintenance of crypts	LGR5, Olmf4, Ascl2, Smoc2, Sox9	[24, 27]
+4 cells	Crypt	Reserve/quiescent ISC population. Replenishes active stem cell population after injury	Bmi1, Tert1, Hopx and Lrig1	[24, 27]
TA cells	Crypt	Forms the intermediate progenitor pool. Differentiate into intestinal cells of secretory or absorptive lineages	DCAMKL1, Lrig1	[27–30]
Paneth cells	Crypt	Secretion of antimicrobial proteins (lysozyme, α-defensins, C-type lectins, and phospholipase A2). Provides necessary biochemical stimuli (Wnt, EGF, and Notch ligands) as well as essential nutrients for the maintenance of ISCs	Lysozyme, α-defensins	[24, 31, 32]
Tuft cells	Crypt and villus	Involved in chemosensing. Regulate type 2 immune response. Has a specific role in the detection of infection by parasitic helminths	Dclk1,Vil1, Pou2f3, α-gustducin, IL-25, TRPM5, Cox-1, Cox-2	[7, 33]
Enteroendocrine cells	Crypt and villus	Involved in chemosensing. Regulate appetite, glucose level, intestinal motility, digestion, and even immune response (via secretion of peptide hormones including somatostatin, CCK, GIP, GLP-1, GLP-2, motilin, neurotensin, secretin, 5-HT, etc.)	Chromogranin A	[34–36]
Goblet cells	Crypt and villus	Protects against bacteria by the production of mucus. Modifies T cell-mediated immunity (via secretion of resistin-like molecule β). Aid in the restoration of epithelia post-mucosal injury (via secretion of trefoil factor). Involved in antigen uptake and presentation to subepithelial dendritic cells. The produced mucus also lubricates the gastrointestinal tract	MUC2, MUC5AC, MUC5B, MUC1, MUC3, MUC17, Tff3	[4, 32, 36–38]
Enterocytes	Villus	Involved in nutrient uptake, trans- or paracellular transportation of macromolecules. Secretion of antimicrobial proteins. Regulate immune response (antigen processing and presentation). Maintains homeostasis between host tissues and intestinal microbial communities (via secretion of IgA). Regulate inflammatory responses (via detoxification of LPS by ALP enzyme)	ALP, maltase glucoamylase, sucrase isomaltase, carbonic anhydrase II	[32, 36, 39–41]
M cells	Peyer's patches and isolated lymphoid follicles	Involved in transepithelial transport of intact microbe and luminal antigens for presentation to the immune cells	Glycoprotein 2, Uromodulin, PrPC, ANXA5	[32, 42, 43]

LGR5 Leucine-rich-repeat-containing G-protein-coupled receptor-5, *Olmf4* olfactomedin 4, *Ascl2* achaete-scute complex homolog 2, *Smoc2* secreted modular calcium binding protein-2, *Sox9* SRY-box, *Bmi1* B lymphoma Mo-MLV insertion region 1 homolog, *Tert1* telomerase reverse transcriptase, *Hopx* homeoboxdomain-only protein, *Lrig1* leucine-rich repeats and immunoglobin-like domains-protein 1, *DCAMKL1* doublecortin- and calmodulin kinase-like 1, *Wnt* wingless-related integration site, *EGF* epidermal growth factor, *Dclk1* doublecortin-like kinase 1, *Vil1* villin 1, *Pou2f3* pou domain, class 2, transcription factor 3, *IL-25* interleukin 25, *TRPM5* transient receptor potential cation channel, subfamily m, member 5, *Cox-1* cyclooxygenase 1, *Cox-2* cyclooxygenase 2, *CCK* cholecystokinin, *GIP* gastric inhibitory polypeptide, *GLP-1* glucagon-like peptide 1, *GLP-2* glucagon-like peptide 2, *5-HT* 5-hydroxytryptamine, *MUC2* mucin 2, *MUC5AC* mucin 5, subtypes A and C, *MUC5B* mucin 5, subtypes B, *MUC1* mucin 1, *MUC3* mucin 3, *MUC17* mucin 17, *Tff3* trefoil factor 3, *LPS* lipopolysaccharides, *ALP* alkaline phosphatase, *PrPC* cellular prion protein, *ANXA5* annexin A5

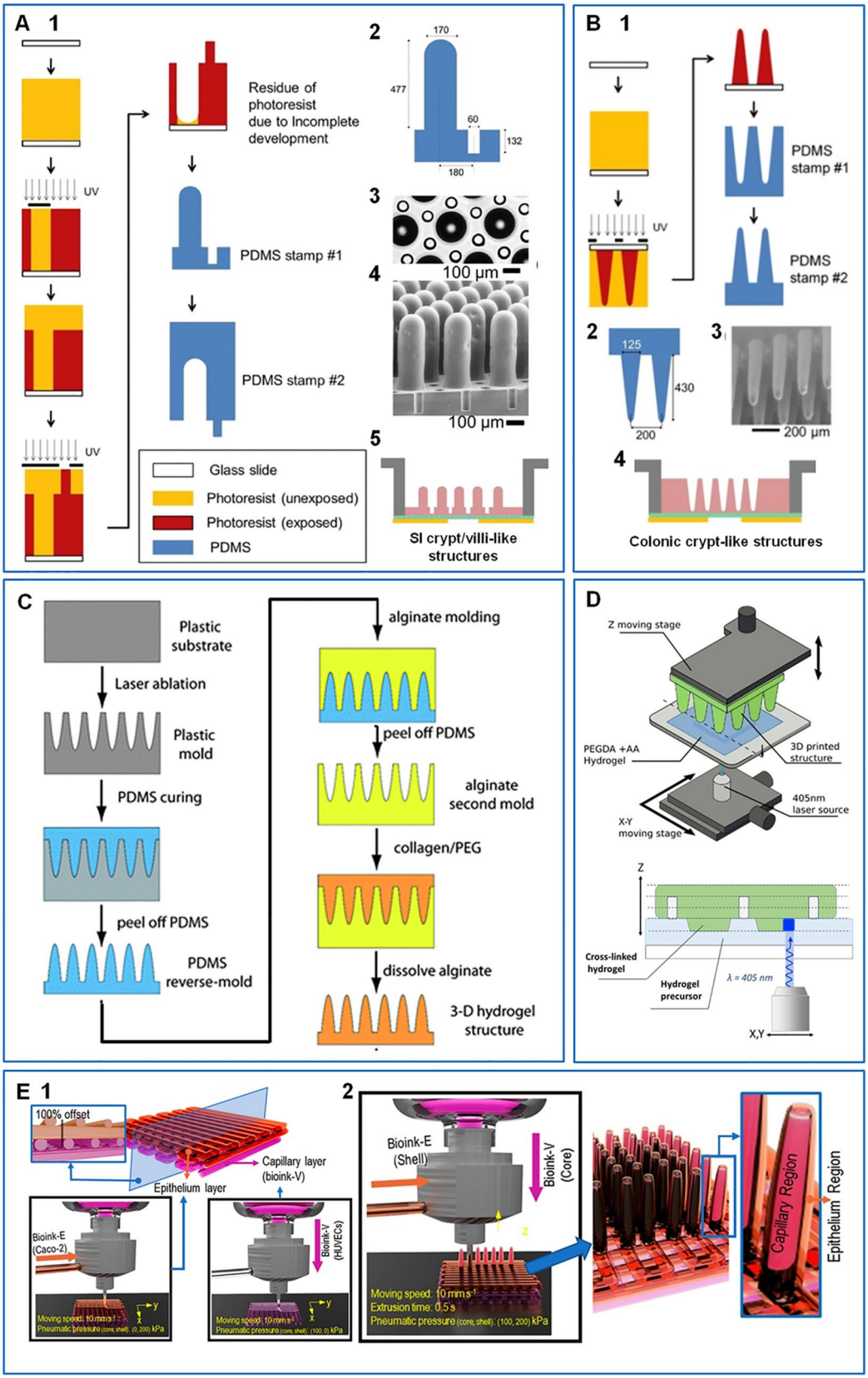
A
1
UV
UV
Residue of photoresist due to Incomplete development
PDMS stamp #1
PDMS stamp #2
Glass slide
Photoresist (unexposed)
Photoresist (exposed)
PDMS
2
170
477
60
132
180
3
100 μm
4
100 μm
5
SI crypt/villi-like structures
B
1
UV
PDMS stamp #1
PDMS stamp #2
2
125
430
200
3
200 μm
4
Colonic crypt-like structures
C
Plastic substrate
Laser ablation
Plastic mold
PDMS curing
peel off PDMS
PDMS reverse-mold
alginate molding
peel off PDMS
alginate second mold
collagen/PEG
dissolve alginate
3-D hydrogel structure
D
Z moving stage
PEGDA +AA Hydrogel
3D printed structure
405nm laser source
X-Y moving stage
Z
Cross-linked hydrogel
Hydrogel precursor
λ = 405 nm
X,Y
E
1
100% offset
Capillary layer (bioink-V)
Epithelium layer
Bioink-E (Caco-2)
Bioink-V (HUVECs)
2
Bioink-E (Shell)
Bioink-V (Core)
Moving speed: 10 mm·s⁻¹
Extrusion time: 0.5 s
Pneumatic pressure (core, shell): (100, 200) kPa
Capillary Region
Epithelium Region

◂**Fig. 2** Fabrication strategies. **a** Two-layer photolithography to replicate crypt-villi features. **1** The fabrication process of PDMS stamps. **2** Measurement specifications the developed PDMS stamp #1. Values mentioned in µm. **3** Bright-field micrographs of the stamp #1 from the top-view. **4** Scanning electron micrographs of stamp #1 from the side view. **5** Schematic representation of the SI-associated patterns developed on collagen scaffolds in the modified transwell insert. Reprinted with permission from [48]. **b** Single-layer photolithography to replicate colonic crypt features. **1** The fabrication process of PDMS stamps. **2** Measurement specifications the developed PDMS stamp #2. Values mentioned in µm. **3** Scanning electron micrographs of the PDMS stamp #2. **4** Schematic representation of the colon-associated crypt structures developed on collagen scaffolds in the modified transwell insert. Reprinted with permission from [46]. **c** Fabrication steps to obtain 3D collagen villi-like structures, starting from a plastic substrate created by laser ablation from which the PDMS mold and then alginate mold are replicated. The alginate mold is finally dissolved. Reprinted with permission from [51]. **d** Schematic representation of SLA strategy for layer-by-layer fabrication of 3D printed PEGDA scaffolds (in the presence of a photoinitiator and AA polymer chains) using a 405 nm laser. Reprinted with permission from [58]. **e** Extrusion-based bioprinting strategy. Representative schematics of the fabrication process of **1** 2D mesh-like crypts and **2** 3D finger-like villi. Two bioinks, namely bioink-E (with Caco-2 cells) and bioink-V (with HUVEC) were employed. The villus architecture consisted of inner vascular core (bioink-V) and an exterior shell of epithelial cells (bioink-E), developed using VMEPS with core–shell nozzle. Reprinted with permission from [62]

UV laser ablation was used to develop plastic molds with high-aspect-ratio holes. The features were replicated on PDMS and on calcium alginate that was subsequently dissolved to achieve final 3D collagen/PEG villus-like structures. The use of calcium alginate as a sacrificial mold eliminated the stress associated with the separation of the mold from the hydrogel structure, enabling the fabrication of patterns with high aspect ratio and curvature, without damaging them (Fig. 2c) [51]. Similarly, CO_2 laser was also employed for developing poly(methyl methacrylate) (PMMA) templates and subsequently 3D patterned collagen scaffolds [52, 53]. The CO_2 laser system is often advantageous than UV laser for developing molds with high aspect ratios due to its higher etching capability.

Porous PLGA scaffolds were produced by a modified version of the porogen leaching-thermally induced phase separation method. PLGA was mixed with sodium bicarbonate as a porogen, and the solution was poured into the agarose molds. After PLGA casting, the scaffolds were frozen at -20 °C, submerged in pre-cooled ethanol to extract chloroform and finally immersed in warm distilled water to dissolve the porogen [54]. In another study, the same strategy was employed to develop porous 3D patterned scaffolds with poly-ethylene-co-vinyl-acetate (PEVA) polymer [55].

Although the substrates mimicking crypt-villus geometry have widely been fabricated using the above-mentioned strategies, the obtained microstructures are only an approximation of the irregular and multiscale topography of the native tissue. To enable the polymeric replica of biomimetic irregular SI geometries, chemical vapor deposition (CVD) of Parylene C on decellularized porcine SI was introduced [56]. After Parylene C was deposited, the porcine tissue was removed by bleach immersion. The side of the material, in contact with the tissue, contained the negative pattern of the native intestine and was used as a mold to prepare a PDMS replica. Resulting PDMS substrates exhibited multiscale resolution features, including crypt-villi structures and the underlying basement membrane [56].

3D bioprinting

3D printing or additive manufacturing involves the fabrication of 3D objects by layer-by-layer deposition of material(s), following a computer-aided design (CAD) model [57]. Recently, stereolithography (SLA), a form of 3D printing, was employed to fabricate artificial scaffolds matching the topography and dimensions of the mouse intestinal epithelium with a microscale resolution (Fig. 2d) [58]. The authors employed the same PEGDA-AA-based polymeric formulation, similar to that used in the other study [49]. The printed scaffolds were further conjugated with ECM proteins (fibronectin or laminin or collagen) to improve its suitability for cell culture. Notably, unlike the previous study which used photolithography to fabricate villi-like structures with PEGDA-AA formulation [49], implementation of 3D printing offered more uniformity in the printed structures as well as allowed to develop scaffolds with both crypts and villi geometries [58].

Further, the advanced versions of 3D printing even allow fabrication of cell-laden 3D constructs, which is otherwise difficult to achieve with traditional ones. They often use a bioink formulation consisting of cells and cell-protecting hydrogels. Moreover, this strategy can enable the printing of multiple cells in the desired region within the scaffold [59, 60]. In this regard, 3D bioprinting was employed to mimic the human intestinal villi with Caco-2 cell-laden collagen bioink, crosslinked with tannic acid, a natural polyphenol. The bioprinting process involved two steps: (i) printing of a flat mesh structure to fabricate the crypt region and (ii) printing in the vertical direction by a vertically moving extrusion-based printing system (VMEPS) to obtain a protruded villus structure [61].

The same group introduced a dual-cell printing system supplemented with a core–shell nozzle to fabricate 3D intestinal villi containing epithelium as well as a blood capillary network (Fig. 2e). They prepared two bioinks: bioink-E with Caco-2 cells, for shell region, and bioink-V with human umbilical vein endothelial cells (HUVECs) for the core region. This time, the process involved three steps: (1) printing of a layer of flat mesh structure using bioink-V; (2) printing of a second layer using bioink-E on the bioink-V

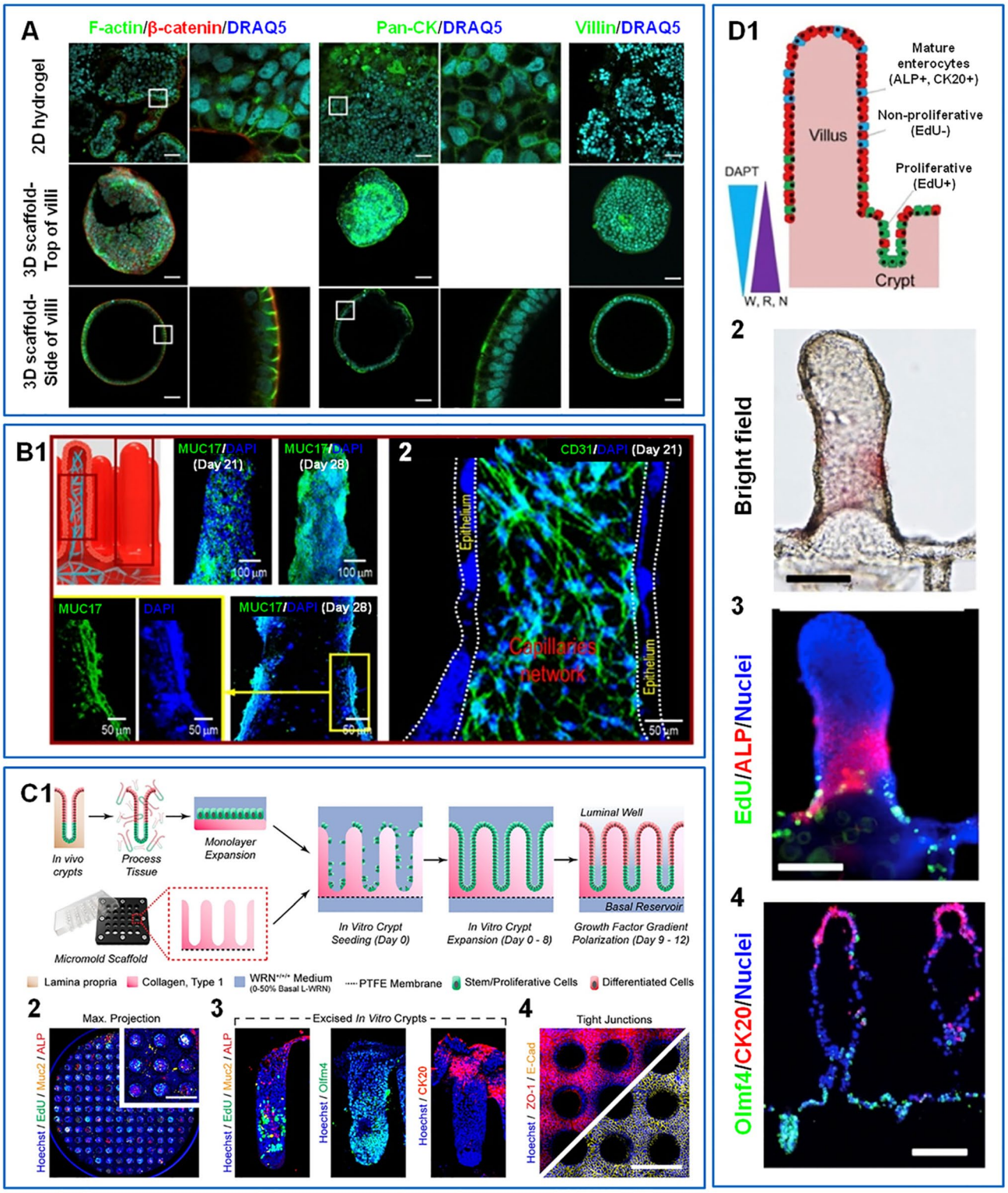

structures with 100% offset; and (3) the villus-like structures were obtained by simultaneously printing bioink-E and bioink-V in the vertical direction using a core–shell nozzle [62]. The same strategy was further opted to develop 3D intestinal patterns using collagen/decellularized porcine SI submucosa-based bioinks [63].

◂**Fig. 3** Cell responses on the 3D intestinal models. **a** Representative confocal micrographs of Caco-2 cells cultured on 2D hydrogels and 3D SLA-printed scaffold (at the top and side of a villus) for 21 days. Expression and distribution of F-actin/ Pan-cytokeratin/villin are shown in green, β-catenin in red, and the nucleus is stained blue with DRAQ5 (Scale bar 50 μm). White square mark the area zoomed for better visualization; images provided in the right-hand side of each subset. Reprinted with permission from [58]. **b** Representative immunofluorescence micrographs demonstrating the presence of **1** MUC17+Caco-2 cells (at the exterior) and **2** CD31+capillary-like network (in the core) in the bioprinted intestinal model. Nucleus was stained with DAPI. Reprinted with permission from [62]. **c** Generation of colonic crypts. **1** Schematics of the culture of colon-derived crypt cells on micromolded collagen scaffold. Post-seeding on the scaffolds, the crypt cells were expanded till day 8. Cellular differentiation and polarization were induced via exposure to growth factor gradient. Representative images demonstrating spatial expression of intestinal markers in colonic crypts differentiated in vitro in the **2** top-view (max projection along the z-axis and summing up the images) and **3** side view. **4** Confocal micrographs showing expression of ZO-1 and E-cad at the luminal surface of the differentiated in vitro crypts. Reprinted with permission from [47]. **d** Generation of SI-associated crypt-villus pattern in vitro. **1** Illustration showing the effect of combined WRN growth factors and DAPT gradient on cell polarization. **2** Bright-field images of the cell-seeded 3D structure (Scale bar 100 μm). Representative images, demonstrating the distribution of **3** EdU/ALP and **4** Olfm4/CK20 positive cells along with the 3D pattern with nucleus stained in blue (Scale bar 100 μm). Reprinted with permission from [48]

Functional behavior of the cells on 3D intestinal models

Gene expression and barrier functions

Substrate topography plays a fundamental role in determining the physiological function of a variety of cell types including osteoblasts [64], hepatocytes [65], cardiomyocytes [66], and even stem cells [64]. It influences cell–matrix interaction, cell–cell interaction, and biomechanical cues, modulating the intracellular signaling cascade, and subsequently, the cell behavior [52]. Intestinal cells are no different in this regard.

A notable difference between that arises due to the presence of villus-like structures is the available surface area for cellular growth that may influence their physiological behavior. A study demonstrated that cells on both 2D and 3D models grew at a similar rate for the first 12 days, but after 16 days, they had grown twice on patterned 3D substrates. Additionally, a decrease in TEER values (i.e., the integrity of tight junctions formed by cell–cell contacts) and an increase in absorptive permeability of fluorescein could be attributed to an increase in culturable surface area. A reduction in the expression of occludin and p-glycoprotein (P-gp, an efflux transporter protein) was also evident as compared to the 2D model. Metabolic enzymatic activities associated with intestinal epithelium were also evaluated; ALP and cytochrome P450 3A4 (CYP3A4) activities were higher in the 3D models, while ANPEP activity was comparable in both of them [67]. In a different study, cell monolayer grown on villi-like 3D collagen constructs presented TEER values that more closely correlated with the in vivo intestine, than on the traditional 2D models. Drug permeability tests with Atenolol showed ~ 13 times higher permeability coefficient in the 3D patterned constructs compared to 2D ones [53].

3D topological features also affected the differential phenotype in a spatial manner. Poly-ε-caprolactone (PCL)/PLGA 3D patterned membranes facilitated differentiation of Caco-2 cells, as evidenced by the brush-bordered cell phenotype (at the top of the villus), temporal increase in the activity of (ALP) during differentiation, and uniform zonula occludens-1 (ZO-1) expression. Lower TEER, along with higher uptake of ^{25} Mg and ^{45}Ca, was witnessed on the 3D membranes as compared to the non-patterned 2D ones [68]. In another study, Caco-2 cells seeded onto PEGDA-AA 3D scaffolds showed directional migration from the base to the top of the villus, to fully cover them. After 21 days, Caco-2 cells expressed markers such as villin (at the apical side of the microvilli), ZO-1 (in tight junctions), and β-catenin (in the basolateral cell membranes). The 3D villi-like constructs had lower TEER values and higher permeability coefficient than the conventional Transwell controls [49].

Recently, printed PEGDA-AA-fibronectin hydrogel scaffolds, 2D and 3D, were used to study the impact of 3D topography on Caco-2 differentiation. 2D coverslip (with or without fibronectin coating) was also taken as 2D control. Cells formed a confluent monolayer in all three surfaces; however, there existed significant differences in their phenotypic characteristics. The cells on glass coverslip exhibited flattened morphology without any apicobasal polarization, irrespective of fibronectin coating. On the contrary, elongated morphology and polarized cells were observed on the printed hydrogel matrices, both 2D and 3D. Cells on the 3D scaffolds demonstrated higher cell elongation, better cell polarity, and higher expression of villin and ALP, as compared to 2D hydrogels. The study also revealed that the height of the villus (500 or 1500 μm) did not critically affect cell polarization (Fig. 3a) [58].

As mentioned above, intestinal epithelium harbors multiple cell types. Thus, to better mimic cellular profiles, existing in vivo, Caco-2 and HT29-MTX were cocultured on porous PLGA scaffolds in a 3:1 ratio. A directional cellular migration from the base to the top of the scaffold was evident, with villus tips having better differentiated phenotypic characteristics. Higher ALP secretion and mucus production, along with lower TEER values, were observed in 3D constructs than their 2D counterparts [54]. Integration of native-like vascular network is necessary, yet challenging aspect for developing the intestinal model. In this regard, the coaxially 3D printed models with spatially defined localization

of Caco-2 (at the exterior) and HUVEC (in the core) were shown to support an improved differentiated phenotype of the epithelial cells, in terms of ALP and ANPEP activity, expression of MUC17, and the presence of brush-border epithelium, as compared to the models without HUVEC. Besides this, HUVEC also underwent a transition to form a capillary-like network in coculture models (Fig. 3b) [62].

Intestinal models are also applied for ascertaining the role of the microbial population (both healthy gut microbes and pathogenic ones) in the gut. The conventional 2D models fall short in mimicking the original bio-interactive profiles of the intestinal epithelium with the microbes. A recent study highlighted a lower invasion by pathogenic bacterial strains, *Escherichia coli* O157: H7 and *Salmonella typhimurium* on 3D patterned scaffolds. Such an outcome was linked to higher expression of mucin-related genes, particularly MUC17, in the case 3D substrates than the 2D monolayer cultures [52].

Intestine-associated cellular compartmentalization

Although the studies mentioned in the previous section demonstrate physiologically relevant spatially discrete phenotypic features, they fail to closely recapitulate the aspects of native-like cellular compartmentalization. The intestinal epithelium has a distinct crypt-villus (in SI) or crypt-lumen (in LI) architecture; wherein stem cell niche lies in the crypts, while the differentiated polarized cells are present at the villus/luminal surface [69]. Current efforts to recapitulate such complexity utilize gradient of growth factors and small molecules across the 3D patterned scaffolds, seeded with intestinal crypt cells, which drives migration and differentiation process, creating lineage compartmentalization, similar to the native tissue.

In this regard, collagen-coated microhole array was fabricated for reproducing the cell compartmentalization in crypt structures. Primary mouse colon crypt cells were seeded, and localized gradients of growth factors (Wnt3A, R-spondin, Noggin; together termed as WRN) were applied across the microholes, thereby yielding a stem/proliferative region (5-ethynyl-2′-deoxyuridine (EdU)+) inside the microholes, and non-proliferative and differentiated (ALP+) zones distant from the microholes [20]. Another crypt-lumen model was fabricated to study intestinal cell compartmentalization process, where human intestinal crypt cells were cultured on a micromolded collagen scaffold (with an array of crypt-like invaginations) and subjected to a biochemical gradient by placing WRN-rich medium in the basal reservoir and WRN-deficient medium in the upper (or luminal) reservoir. Polarization of the in vitro tissue was observed with proliferative cells (EdU+, olfactomedin 4 (Olfm4)+) in the crypt region and differentiated cells (EdU+, keratin 20 (CK20)+ and erzin+) at the luminal surface. Interestingly, mucus-secreting goblet cells (MUC2+) were also observed [46].

Scalability of the intestinal model is one of the most pertinent challenges. In this regard, a scalable platform consisting of ~ 3875 crypts over a single membrane, where chemical gradients could be simultaneously imposed in distinct regions; this enables a parallelizable in vitro crypt formation system. Here also, crypts were seeded with human colon crypt cells, and exposure to WRN gradients resulted in cellular compartmentalization. Proliferative cells (EdU+, Olfm4+) were restricted to the basal region of the crypts, whereas differentiated colonocytes (ALP+, CK20+) were present at the luminal plane. Proteins responsible for tight and adherens junction maintenance such as ZO-1 and E-cadherin (E-cad) were displayed at the luminal plane. Goblet cells were also present (Fig. 3c) [47].

Besides, in a more recent study, the conventional WRN-gradient (basal to luminal) was found to be insufficient to fully induce cellular compartmentalization on 3D collagen constructs, seeded with human small intestinal crypt cells. Incorporation of the second gradient of a small molecule, DAPT (luminal to basal), overcame this issue. After applying a dual gradient strategy, proliferative (EdU+, Olfm4+) and differentiated (CK20+, ALP+) cells were observed explicitly in crypt and villus regions, respectively. Moreover, EdU+ cells migrated upwards along the crypt-villus axis over time, similar to in vivo (Fig. 3d) [48].

These studies indicate that mimicking the 3D geometry of the intestinal epithelium influences the cellular phenotype. Table 2 summarizes all the studies that have evaluated cellular behavior on a 3D microstructured construct to date.

Modulation of intestinal cell behavior: biophysical and biochemical determinants

Controlling the in vitro behavior of the cells (both the stem cells and differentiated ones) and achieving desirable in vivo-like effects, are some of the biggest challenges faced by the researchers. The recent understanding of existing multifactorial determinants (intrinsic and extrinsic) of cell behavior has led to significant advancements in this field. Principally, the biochemical nature of in vivo ECM is mimicked, by utilizing in vivo-like mechanical and physical cues that have now been established as substantial regulation factors of cell fate and behavior. Moreover, recreating the cellular environment and interactions with neighboring cell population and intestinal microflora has also being explored. Besides, creating various gradients of ECM components, biochemical factors, and gases, similar to the native crypt-lumen (in LI) and crypt-villus (in SI) axis are also pertinent options (Fig. 4).

Table 2 Additional studies on in vitro intestinal tissue model with patterned crypt-villus geometry

3D architectural features	Fabrication methodology used	Material used	Specifications of crypts or villi or both			Cells used	Gene/protein expression or activity in 3D (v/s 2D)	Compartmentalization	$TEER_{3D}$ (v/s $TEER_{2D}$) (in Ω cm^2)	Absorptive P_{3D} (v/s P_{2D}) (in cm/s)	Secretive P_{3D} (v/s P_{2D}) (in cm/s)	Time before experimental analysis (days)	References
			Villus	Crypt	Crypt-villus					Metabolite analyzed (Values)	Metabolite analyzed (Values)		
Intestinal crypt configuration	Photolithography	Collagen	–	Diameter: 50 µm	–	Murine intestinal crypts	ALP, MUC2 (not compared with 2D)	Crypt: EdU+; zones distant from crypts: ALP+, MUC2+ goblet cells were observed near the crypt microholes	–	–	–	4	[20]
	Photolithography and replica molding	Collagen (crosslinked with EDC/NHS)	–	Depth: 430 µm; base diameter: 125 µm (at the base); density: 35/mm^2	–	Human colonic crypts	CK20, Olfm4, Erzin, MUC2 (not compared with 2D)	Crypt: EdU+, Olfm4+; Luminal plane: CK20+, Erzin+; MUC2+ goblet cells were also observed	–	–	–	12 (extendable to atleast 32)	[46]
	Photolithography and replica molding	Collagen I hydrogel (EDC/NHS crosslinking)	–	Depth: 250 µm; diameter: 75 µm	–	Mouse colonic epithelial cells	Sox9-EGFP, ALP, MUC2 (not compared with 2D)	Crypt base: EdU+,Sox9+; Luminal plane: ALP+	–	–	–	4	[70]
	Photolithography and replica molding	Collagen (crosslinked with EDC/NHS)	–	Depth: 419.1 µm; diameter: 65.4 µm (at the base); diameter: 128.1 µm (lumen)	–	Primary human colon epithelial cells	E-cad, ZO-1, CK20, MUC2, ALP, Olmf4 (not compared with 2D)*	Crypt: EdU+, Olfm4+; Luminal plane: ALP+, CK20+, ZO-1+, E-cad+; MUC2+ goblet cells were also present	–	–	–	12	[47]
Intestinal villus configuration	Laser ablation of PMMA and replica molding	PGS (along with a sodium bicarbonate as porogen; crosslinked with MDI)	Height: 340 µm; width: 184.5 µm (at the base) to 49 µm (at the tip); spacing: 69.5 µm	–	–	Caco-2 or juvenile mouse small intestinal crypt cells	CrgA, SI, E-cad (not compared with 2D)	–	–	–	–	7	[21]
	Laser ablation of PMMA and replica molding	Collagen or PEGDA	Height: 450–500 µm; aspect ratio: ~ 5	–	–	Caco-2	–	–	–	–	–	7–10	[51]

Table 2 (continued)

3D architectural features	Fabrication methodology used	Material used	Specifications of crypts or villi or both			Cells used	Gene/protein expression or activity in 3D (v/s 2D)	Compartmentalization	TEER$_{3D}$ (v/s TEER$_{2D}$) (in Ω cm^2)	Absorptive P_{3D} (v/s P_{2D}) (in cm/s) Metabolite analyzed (Values)	Secretive P_{3D} (v/s P_{2D}) (in cm/s) Metabolite analyzed (Values)	Time before experimental analysis (days)	References
			Villus	Crypt	Crypt-villus								
	Laser ablation of PMMA and replica molding	PLGA (along with a sodium bicarbonate as porogen). Scaffolds were coated with Matrigel for the culture of intestinal crypts	Height: 500 µm; diameter: 200 µm (at the base); pore size: 5–10 µm	–	–	Caco-2 and HT29-MTX (3:1) or mouse small intestinal crypt cells	Increased: ALP activity and mucus production	Villus tip: Well differentiated cells; Base: Low cell differentiation	290 (v/s 710 for polycarbonate membrane)	–	–	21	[54]
	Laser ablation of PMMA and replica molding	Collagen (crosslinked with glutaraldehyde)	Height: 565 µm; density: 25/mm^2	–	–	Caco-2	–	Villus tip: More polarized and columnar cells; Base: Low cell polarization	40 (v/s 170 for collagen membrane and 260 for polycarbonate membrane)	Antenolol: 0.912×10^{-5} (v/s 0.07×10^{-5} for collagen membrane and 0.058×10^{-5} for polycarbonate membrane)	–	14	[53]
	Laser ablation of PMMA and replica molding	Collagen	Height: 400 µm; diameter: 200 µm (at the base); density: 25/mm^2	–	–	Caco-2	Increased: MUC17	–	90 (v/s 260 for polycarbonate membrane)	FITC dextran (4 kDa): 1.5×10^{-6} (v/s 0.7×10^{-6} for polycarbonate membrane)	–	20	[52]
	Photolithography	PEGDA-AA (functionalized with laminin or collagen type I via EDC/NHS crosslinking)	Height: 440 µm, diameter: 85 µm (at the tip)	–	–	Caco-2	Villin, ZO-1, and β-catenin (not compared with 2D)	–	290 (v/s 3500 for polycarbonate membrane)	FITC dextran (4.4 kDa): 1.5×10^{-6} (v/s 0.2×10^{-6} for polycarbonate membrane)	–	21	[49]
	Photolithography and sacrificial etching	SU-8	Different height, cross-sectional area, and spacing	–	–	Caco-2	Occludin (no comparison shown)	–	–	–	–	21	[71]
	Photolithography and replica molding	Collagen	Height: 300 µm; aspect ratio: 4–5	–	–	Caco-2	Increased: CYP3A4, ANPEP, and ZO-1; Decreased: P-gp	–	–	Fluorescein: 7.38×10^{-6} (v/s 1.71×10^{-6} for polycarbonate membrane); Rhodamine 123: 4.93×10^{-6} (v/s 2.62×10^{-6} for polycarbonate membrane)	Rhodamine 123: 1.15×10^{-6} (v/s 2.26×10^{-6} for polycarbonate membrane)	14	[72]

Table 2 (continued)

3D architectural features	Fabrication methodology used	Material used	Specifications of crypts or villi or both			Cells used	Gene/protein expression or activity in 3D (v/s 2D)	Compartmentalization	$TEER_{3D}$ (v/s $TEER_{2D}$) (in $\Omega\ cm^2$)	Absorptive P_{3D} (v/s P_{2D}) (in cm/s)	Secretive P_{3D} (v/s P_{2D}) (in cm/s)	Time before experimental analysis (days)	References
			Villus	Crypt	Crypt-villus					Metabolite analyzed (Values)	Metabolite analyzed (Values)		
	Photolithography and replica molding	Collagen (crosslinked with glutaraldehyde)	Height: 400 µm; diameter: 100 µm (at the base); surface area 0.1 mm^2	–	–	Caco-2	Decreased: P-gp and ZO-1	–	60–80 (v/s 200 for polycarbonate membrane)	FITC-dextran (4 kDa): 1.5×10^{-6} (v/s 0.78×10^{-6} for polycarbonate membrane); fluorescein: 9.1×10^{-6} (v/s 7.1×10^{-6} for polycarbonate membrane)	Rhodamine-123: 2.9×10^{-6} (v/s 4.3×10^{-6} for polycarbonate membrane)	20	[67]
	Photolithography and replica molding	PLA	Height: 420 µm; base diameter: 130 µm; density: 32.5/mm^2	–	–	Caco-2	–	–	–	–	–	–	[50]
	Photolithography and replica molding	PCL and PLGA blend	Height: 500 µm; diameter: 450 µm (at the base) to 400 µm (at the tip); spacing: 80 µm; density: 5/mm^2	–	–	Caco-2	Increased: ALP	Villus tip: More ZO-1 expression, clear microvilli projections; Base: Less defined microvilli projections with low ZO-1 expression	85 (v/s 176 for non-patterned membrane and 215 for polycarbonate membrane)	Fluorescein: 4.378×10^{-6} (v/s 8.756×10^{-6} for non-patterned membrane and 1×10^{-6} for polycarbonate membrane)	–	21	[68]
	Digital light processing stereolithography	GelMA and PCL-MA (photocrosslinked)	Height: 1000 µm	–	–	Caco-2	ZO-1 (no comparison shown)	–	–	–	–	10	[73]
	3D printing and replica molding	PLGA	Height: 1000 µm; diameter: 700 µm (at the base) to 500 µm (at the tip)	–	–	intestinal epithelial cells (IEC6)	–	–	–	–	–	7	[74]
	Vertically moving extrusion-based cell printing	Collagen/decellularized SI submucosa (crosslinked with tannic acid)	Height: 831.1 µm, diameter: 190.9 µm; aspect ratio: 4.4	Mesh (0/90 struts)	–	Caco-2 and HUVEC	ZO-1, E-cad, MUC17, ALP, and ANPEP (not compared with 2D)	–	–	FITC-dextran (4 kDa): 1.44×10^{-6}	–	20–21	[63]
	Vertically moving extrusion-based dual cell printing	Collagen-Based Bioink (crosslinked with tannic acid)	Height: 770 µm; diameter: 183 µm; aspect ratio:4.2	Mesh (0/90 struts)	–	Caco-2 and HUVEC	E-cad, ZO-1, MUC17, ALP, ANPEP (not compared with 2D)*	–	–	FITC-dextran (4 kDa): 0.622×10^{-6} (mesh); 1.889×10^{-6} (villi)	–	14–21	[62]

Table 2 (continued)

3D architectural features	Fabrication methodology used	Material used	Specifications of crypts or villi or both			Cells used	Gene/protein expression or activity in 3D (v/s 2D)	Compartmentalization	$TEER_{3D}$ (v/s $TEER_{2D}$) (in Ω cm^2)	Absorptive P_{3D} (v/s P_{2D}) (in cm/s)	Secretive P_{3D} (v/s P_{2D}) (in cm/s)	Time before experimental analysis (days)	References
			Villus	Crypt	Crypt-villus					Metabolite analyzed (Values)	Metabolite analyzed (Values)		
	Vertically moving extrusion-based cell printing	Collagen (crosslinked with tannic acid)	Height: 708 µm; diameter: 162 µm; aspect ratio: 4.4	Mesh (0/90 struts)	–	Caco-2	MUC17, ALP, and E-cad (not compared with 2D)	–	–	–	–	21–30	[61]
Intestinal crypt-villus configuration	Laser ablation of PMMA and replica molding	PLGA (along with a sodium bicarbonate as porogen)	Height: 500 µm	–	–	Caco-2	–	Villus tip: differentiated cells; Base: undifferentiated cells	449.18 (not compared with 2D)	–	–	21	[75]
	Photolithography and replica molding	Collagen (crosslinked with EDC/NHS)	Height: 477 µm; diameter: 170 µm	Height: 132 µm; diameter: 60 µm	Total mucosal thickness: 609 µm; crypt:villus ratio: 2; each villus surrounded by 6 crypts	Human small intestinal crypts	CK20, ALP, and Olfm4 (not compared with 2D)	Villus: EdU-, ALP+, CK20+; Crypt: EdU+, Olfm4+	–	–	–	9–12	[48]
	High-resolution stereolithography 3D printing	PEGDA-AA (containing fibronectin)	Height: 500 µm; diameter: 300 µm (at the base) to 150 µm (at the tip)	Height: 200 µm; diameter: 50 µm	Total scaffold thickness: 750 µm; each villus surrounded by 6 crypts	Caco-2	Pan-cytokeratin, β-catenin, ALP, and villin (not compared with 2D)	Villus tip: More polarized, ALP+, Villin+ cells; Villus base and crypts: Low differentiation observed	–	–	–	9–12	[58]

*Coculture with HUVEC significantly improved the functionality of the tissue constructs

E-cad E-cadherin, *ANPEP* alanyl aminopeptidase, *PGS* poly(glycerol sebacate), *MDI* 4,4′-methylenebis(phenyl isocyanate), *CrgA* chromogranin A, *SI* sucrase isomaltase, *GelMA* gelatin methacryloyl, *PCL-MA* PCL methacrylate, *EDC* 1-ethyl-3-(3-dimethylaminopropyl)-carbodiimide, *NHS* *N*-hydroxysuccinimide, *Sox9* SRY-box 9, *WGA* wheat germ agglutinin, *SGLT-1* sodium-glucose transporter 1, *Glut-2* glucose transporter 2

ECM composition

As the biological milieu surrounding cells, the ECM is a fibrous network of crosslinked proteins and glycosaminoglycans (GAGs) which makes up most of the cellular microenvironments [76]. Highly hydrated, it forms a hydrogel secreted by cells and connects the latter within tissues, and organs with each other. It provides structural and spatial organization to tissue components, protects the cells against mechanical pressures, mediates cellular attachment and also controls downstream signaling cascades that further determine their behavior [77, 78]. Abounding of signaling molecules for the regulation of tissue function and homeostasis, the ECM further translates information by its composition and molecular architecture, overall constituting a dynamic system of macromolecules implicated in tissue development, maintenance, and repair [76, 79, 80]. Continuously degraded and remodeled according to tissue needs [77], the ECM also presents a tissue-specific composition that enables tissue-specific functions.

In the intestinal epithelium, the ECM in the crypt base is preponderantly made up of the isoforms of fibronectins, laminins, collagens, and GAGs [81], suggesting isoform-dependent regulation of the ISC niche. This is further emphasized by the differential distribution of diverse components along the crypt-villus axis, with laminins α1 and α2 abundant in the crypt base, laminins α3 and α5 present in the villus, fibronectins surrounding the crypt, and tenascin found at the base of villus and in the surrounding of crypts [81–84]. Amongst the collagen superfamily, collagen type IV forms a major component of the intestinal basement membrane and is a key regulator of the mechanical microenvironment of the intestinal crypt cells [81, 84]. Besides the biochemical composition, the ECM also directs cell behavior by its selective entrapment of growth factors and chemical stimuli. In fact, among GAGs, heparan sulfate proteoglycan (also known as perlecan) presents the ability to bind various growth factors such as wingless-related integration site (Wnt), Hedgehog, transforming growth factor beta (TGF-β), and fibroblast growth factors (FGF) proteins, thereby contributing to ISC maintenance [81, 84, 85]. Hence, substrate biochemistry has been used to regulate cell behavior in vitro, often detaining a substantial role in optimizing stem cell microenvironment and their differentiation.

In a study, the authors screened various basement membrane ECM proteins and found that collagen IV readily enabled the attachment of mouse intestinal epithelial cells, while collagen I overlay was essential for preserving the Lgr5+ expression (stem cell marker) in the sandwich cultures [86]. Notably, in the case of collagen type IV coating, the cell attachment was mediated by integrin α2β1, and was dependent on the ECM concentration; 100 μg/mL supporting the highest adhesion. In the same milieu, it was reported that the α2β1integrin binding peptide (from collagen I) is indeed determining in the expansion of intestinal organoids under in vitro conditions [87]. Enrichment of soft PEG hydrogels with ECM proteins of the native intestinal crypt, like laminin-111, collagen IV, hyaluronic acid and perlecan enhanced survival and proliferation of mouse ISCs; however, variabilities existed in the colony formation efficiency amongst the individual ECM components [88]. The importance of laminin-111 was further highlighted for the growth and maintenance of epithelial organoids in a defined hydrogel system [89]. Interestingly, the presence of RGD motifs in the matrix was sufficient to maintain ISC colonies, form intestinal organoids, and improve paracellular transportation in the epithelial cells, in a peptide concentration-dependent manner, thereby providing better control over the biochemical environment [88, 90, 91].

Further emphasizing on 3D patterned substrates, a synergistic effect of substrate topology and ECM protein on the phenotypic characteristics of cultured Caco-2 cells was reported [92]. For this, crypt-like collagen microwells, coated with either laminin or fibronectin, were used. The study revealed better cell differentiation characteristics, barrier function, ANPEP, and ALP activity, on laminin-coated substrates than on the fibronectin-coated ones. On the other hand, the topological features affected cell adhesion, spreading and barrier functions. In the same backdrop, a recent study highlighted that adding decellularized SI submucosa to collagen type I-based bioink improves cellular activities in bioprinted Caco-2 cells, allowing for the formation of the more biomimicking intestinal epithelium, aided by a bioengineered villus geometry [63].

Altogether, these findings underline the essential role of matrix biochemistry in modulating intestinal cell growth and differentiation, with ECM proteins conditioning in vitro cell adhesion, proliferation and differentiation.

Matrix stiffness

Among the parameters regulating cellular behavior, substrate stiffness represents one of the most critical factors, controlling cell phenotype and determining stem cell fate [93, 94]. Under in vivo conditions, the collagen content in the intestinal submucosa is 2–4 times higher than that in the mucosa region (that contains the epithelium and displays crypt-villus architecture), pointing out the existence of stiffness gradients between these layers [81]. Thus, various studies have attempted to exploit substrate stiffness in optimizing in vitro intestinal epithelium models. However, the consensus is yet to be reached for optimal stiffness due to the cellular response often being a result of both substrates physical and biochemical properties, with different reports depending on the nature of the matrix material. For instance,

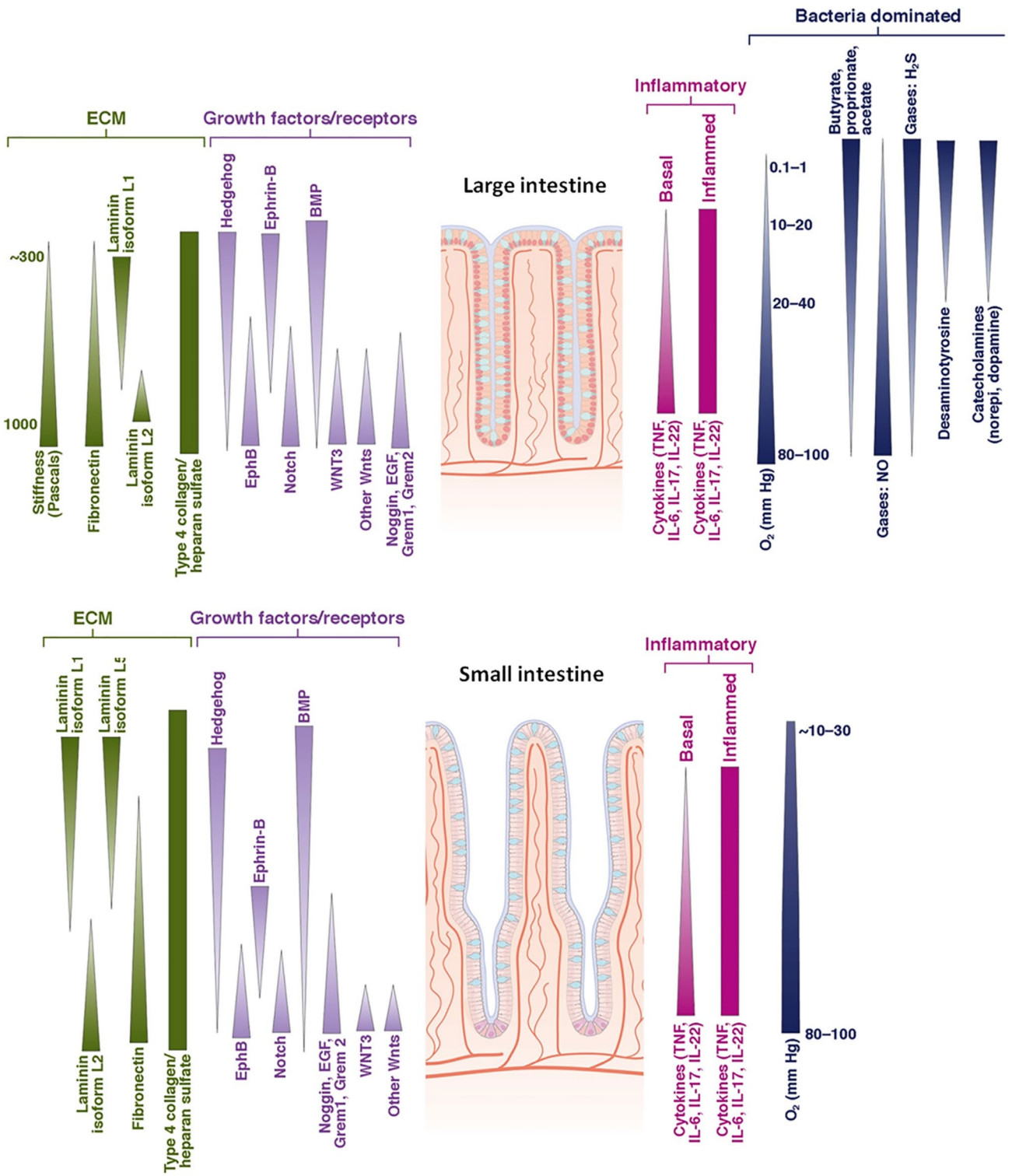

Fig. 4 Illustration of various gradients found along the crypt-lumen (in LI) and crypt-villus (in SI) axis in vivo. Gradients of ECM, growth factors/receptors, inflammatory cytokines, and bacteria-dominated components (gases and small molecules) have been shown with the shades of green, purple, pink, and blue color. The pointing end and the broad base of the triangle represent lower and higher concentration, respectively. Reprinted with permission from [81]

mouse ISCs embedded in PEG hydrogels (conjugated with 1 mM RGD motifs) of higher stiffness (1.3 kPa) supported higher cell proliferation than those with lower stiffness (300 Pa); this involved the yes-associated protein 1 (YAP), a mechanosensing effector and key mediator in ISC self-renewal [88]. In another study, fibrin gels (supplemented with 10% Matrigel) of stiffness range between 77 ± 25 and 140 ± 47 Pa showed higher and bigger cyst formation from mouse ISCs, 4 days post-cell seeding [89]. Similarly, modulation in the matrix stiffness of protein-engineered scaffolds via tetrakis(hydroxymethyl)phosphonium chloride-based crosslinking affected the yield of mouse organoids; softer scaffolds (180 Pa) showed higher organoids formation than the stiffer ones (1220 Pa), irrespective of the content of adhesion motifs [90].

Besides, efforts have been made to create monolayer cultures of intestinal cells that have physiological relevance. Varying stiffness was achieved by simply modulating the thickness of Matrigel coating in polystyrene substrates; with 2.9 ± 0.1 μm (Young's modulus of ≈ 3 GPa) and ~ 2 mm (storage modulus ≈ 50 Pa), thin and thick coatings formed stiff and soft substrates, respectively. Organoid-derived crypts or single cells, when cultured on stiffer substrates underwent spreading and formed epithelial monolayers, whereas those on softer substrates formed organoids [95]. In a separate study, collagen hydrogel substrates with a gradient of stiffness (230 ± 140 Pa) were developed within Transwell inserts using EDC/NHS-mediated gradient crosslinking. The luminal surface with lower stiffness was used for culturing the cells, while the stiff basal surface prevented gel deformation; this closely mimicked the lamina propria of the intestine. The study revealed that lower TEER values along with a higher expression of breast cancer resistance protein (BCRP) and multidrug resistance protein 2 (MRP2) in the case of gradient crosslinked substrates relative to the conventional thinner and stiffer collagen membrane (1.50 ± 0.27 MPa). Moreover, grown primary human small intestinal monolayers enabled prazosin (a substrate of BCRP) transport as in vivo, in contrast with the stiffer substrates [96]. As an extension to this work, the authors demonstrated that the cells on the conventional scaffold lacked various drug-metabolizing enzymes relative to those on the gradient crosslinked hydrogels, additionally not properly responding to known inducers and inhibitors in contrast with the latter substrates [97].

Therefore, substrate stiffness represents an essential factor of cellular microenvironment with potential for directing the behavior of intestinal cells and thus can be leveraged to create more biomimicking in vitro intestinal epithelium models. As to the effect of matrix stiffness in 3D topological constructs, no report is yet available that corroborates the translation of the above stiffness-related findings in such settings, thus extending the scope of future developments.

Shear stress and peristaltic motion

The intestine constitutes a dynamic organ where cells are continuously exposed to peristalsis, an alternation of contraction-relaxation cycles that enable the progression of the luminal content of the hollow organ and facilitate food digestion; notably, differences exist in the flow/transit time and contraction specification of SI and LI [1, 4]. Such microenvironment has been recapitulated in vitro in microfluidic platforms that recreate in vivo cues to affect culture outcome. For instance, using PDMS and soft lithography, a microfluidic device was designed that permitted liquid flow at a low rate (30 μL h^{-1}), producing low shear stress (0.02 dyne cm^{-2}) and cyclic strain of 10% (0.15 Hz), thus reminding physiological peristaltic movements [13]. When Caco-2 cells were cultured therein, compared to static culture in Transwell inserts, the assembled cues led to the growth of a columnar epithelium with improved polarization, paracellular transport, ANPEP activity, and barrier function that further formed intestinal villi-like folds, much like the whole intestine. Moreover, the cells grown under such complex conditions, unlike those under static conditions, maintained their viability and barrier function even when cocultured with a probiotic bacterium, *Lactobacillus rhamnosus* GG. Under similar microenvironmental conditions, the reconstitution of proliferative crypts was highlighted. EdU+ cells further differentiated into enterocytes, goblet, enteroendocrine, and Paneth cells along the crypt-villus axis [98]. Better CYP3A4 activity was also observed. In a recent study, intestinal morphogenesis was shown to be influenced by fluid-flow rates in a time-dependent manner, the flow regime between 70 and 120 μL h^{-1}, being most effective [14]. The authors also identified Frizzled-9 receptor as the mediator of this flow-induced spontaneous morphogenesis. By changing the fluid shear stress from ~0 to 0.03 dyne cm^{-2} (physiological range), it was observed that phenotype of Caco-2 cells (mucus secretion, microvilli formation, expression of tight junctions and CYP3A4) could be modulated, with a shear stress of 0.02–0.01 dyne cm^{-2} creating the optimum parameters [99]. Another study also revealed that the response of intestinal epithelium to strain, in terms of proliferation and activation of downstream signaling cascades, was dependent on ECM proteins. Collagen I, collagen IV, and laminin positively modulated cell proliferation under cyclic strain, but not fibronectin [100]. Interestingly, better tissue growth and maturation were observed when human intestinal organoids, exposed to uniaxial strain, were transplanted in mice mesentery, according to Poling et al. [101] who performed morphometric, transcriptomic, and functional studies on the explanted constructs.

In an attempt to integrate fluid-flow dynamics with intestine-associated topological features, recently, a 3D printed bioreactor was developed [55]. The study revealed the formation of site-specific expression profiles of Caco-2 differentiation with elevated apoptosis at the tip of the villus (regions subjected to the highest shear), and less ALP but increased mucus secretion near the base [55]. These results were more similar to in vivo intestine than those obtained in the case of conventional 2D Transwell culture or static structures. Active glucose transportation (at a higher rate) along with decreased TEER values were also evident in the presence of 3-D topography and fluid-induced shear. In the same prospect, the combination of 3D topology and shear yielded synergistic effects, giving Caco-2 cells an adequate stimulus for differentiation and considerably improving their metabolic activities; specifically, CYP3A4 activity was 7 times higher on 3D scaffold under fluidic condition than static 2D conditions [72]. Also, ANPEP activity and cell absorptive permeability were enhanced in the 3D fluidic conditions.

Given all these regulatory effects, mechanical cues constitute a major factor in the design and fabrication of devices and tissue models aiming to recapitulate the intestinal tissue for various pathophysiological and pharmacological studies.

Coculture with other cell types as well as microflora

Another strategy for biomimicking the physiology of the intestinal epithelium is by coculturing epithelial cells with other impactful cells (including microbial cells) that provide structural support and/or participate in regulatory cross-talks with the cells of interest, via generation of gradients of growth factors, gases, and microbial products, thereby regulating the dynamics of ISC niche and maintenance of intestinal health [81]. Thus, many efforts have been directed toward developing suitable in vitro coculture modules.

In a study, Caco-2/HT29-MTX coculture and Caco-2/HT29-MTX/Raji B triple culture models showed more physiological relevance than Caco-2 monoculture models for studying the intestinal permeability of the drugs [102]. Intestinal muscularis cells were cocultured with intestinal epithelium on collagen-coated PCL tubular scaffolds, showing the presence of 11 different cells types from the mucosa, the muscularis, and the serosa and long-term spontaneous and periodic contractions, thereby recapitulating native-like characteristics, to an extent [103]. Incorporation of human intestinal microvascular epithelial cells with intestinal epithelium in a parallel channel of a microfluidic device (accompanied by flow-induced shear and cyclic strain) enhanced the rate of intestinal morphogenesis compared with those cultured without endothelial cells and showed better resemblance with native human duodenum [104].

One of the most utilized components in coculturing approaches is the addition to epithelial cells of supportive stromal cells, generally fibroblasts or myofibroblasts [105, 106]. The presence of the NIH-3T3 fibroblasts accelerated the formation of epithelial layer by Caco-2 cells, strengthened its barrier function and improved its absorptive permeability as well as promoted the recovery upon disruption of intestinal barrier [105]. Intestinal subepithelial myofibroblasts (ISEMFs) were shown to support the long-term culture of intestinal organoids, even in the absence of a few critical growth factors required for maintaining cultures [107]. Moreover, supplementation of ISEMFs conditioned medium was sufficient to prevent autolysis of human intestinal organoids in collagen gels [108]. Enteric nervous system (ENS) cells have also been utilized to elucidate their interactions with murine ISCs [109]. The findings showed that ENS cells and myofibroblasts together control the stem cell behavior, particularly inducing their differentiation into enteroendocrine cells at a higher proportion relative to that done by coculture with myofibroblasts alone. Moreover, better barrier function and reduced flux of FITC-dextran was also evident in co- or tri-cultured models as compared to mono-cultured ones. Besides this, all three systems also showed variations in the production of cytokines.

Considering the involvement of gut microbiota in the various metabolic processes as well as pathobiological conditions [110, 111], they have also been introduced in various in vitro intestinal models, thereby aiming toward recreating more in vivo-like microenvironment. Coculture of organoids with *Lactobacillus rhamnosus* GG resulted in an increased percentage of proliferative cells and improved differentiation into Paneth cells, while *Lactobacillus reuteri* D8-induced proliferative effects in the organoids and prevented them from the damaged caused by TNF-α [112]. Besides, pathologic bacteria are introduced in intestinal epithelial culture systems to study pathophysiological pathways involved in infections and certain pathological conditions [22, 113]. Here, it is also important to mention that the microbiome products such as polyamines and short-chain fatty acids (SCFAs) also critically determine intestinal dynamics, and thus need consideration. For instance, butyrate, a type of SCFA, is essential for differentiated colonocytes for undergoing healthy mitochondrial respiration and promoting barrier function (at a lower concentration), while it acts as an inhibitor to ISC proliferation [81, 114–116]. Polyamines are essential for the growth and development of intestinal mucosa [81, 117, 118].

Implementation of coculture strategies on the patterned 3D scaffolds also revealed improvements in the functional aspects of the intestinal epithelium (studies discussed in section "Functional behavior of the cells on 3D intestinal models") [54, 62, 63]. Moreover, treatment of butyrate in 3D colonic model inhibited cryptic proliferation, while inducing differentiation into ALP+ absorptive lineage [20, 46, 47].

Exploring avenues in induced pluripotent stem cells (iPSCs)-derived intestinal cells

Intestinal crypts have gained considerable attention for the development of in vitro intestinal tissue models with biomimetic architecture, cellular distribution, and physiological functionality. However, their clinical utility is limited by lack of ideal sources, tedious isolation protocols, the rapid loss of functionality, and existing ethical issues. Therefore, recent research interventions have been directed toward the use of iPSCs, which overcome many of these limitations. Such a strategy has also been advantageous for developing patient-specific intestinal models (healthy/diseased) and corresponding personalized therapies. Moreover, human-specific pharmacokinetic features, closely mimicking the native conditions, could be achieved with the derived intestinal cells, which is otherwise difficult with the available human cell line alternatives. The current section highlights the recent developments in stem cell engineering for deriving intestinal cells. 2D cultures and 3D organoid cultures have majorly been employed for stem cell differentiation and the expansion of intestinal cells; thereafter, these differentiated cells could be harvested and used for different applications including in vitro model development.

In a study, human iPSCs were differentiated into enterocytes-like cells (ELCs) following a step-by-step protocol [119]. iPSCs were first committed toward definite endodermal-like cells (DELCs) lineage using Activin A, followed by differentiation into intestinal progenitor-like cells (IPLCs) using FGF2. The developed IPLCs expressed caudal type homeobox 2 (CDX2, a marker for intestinal development and differentiation) and LGR5 (ISC marker). Further, maturation of IPLCs into ELCs occurred in the presence of epidermal growth factor (EGF) under low serum (2%) conditions. The differentiated cells expressed multiple mature enterocytes markers; however, their expression was relatively lower than adult small intestinal tissue. The study also revealed that Wnt3a treatment had negligible, while FGF4 (instead of FGF2) treatment or the concentration of serum had a pronounced effect on differentiation efficiencies. In an extension to this study, authors conducted iPSCs to IPLCs differentiation following the same Activin A/FGF2 protocol; however, for generating ELCs, different cocktail of small molecules (glycogen synthase kinase 3 inhibitor XV, Dorsomorphin, PD98059, 5-aza-2′-deoxycytidine (5-aza), and A-83-01) were added along with EGF treatment [120]. The study revealed that resultant ELCs exhibited pharmacokinetic functions and showed the expression of mature enterocytes; however, the functional phenotype of the ELCs varied significantly among the treatment groups. In the same backdrop, iPSC-derived DELCs were efficiently differentiated into IPLCs using a cocktail of 6-Bromoindirubin-3′-oxime (BIO) and N-[(3,5-difluorophenyl)acetyl]-*L*-alanyl-2-phenyl-1,1-dimethylethyl ester-glycine (DAPT); meanwhile, further supplementation of SB431542, EGF, and Wnt3A in the culture medium produced ELCs [121]. The generated ELCs exhibited better expression of CYP3A4 and peptide transporter 1 (PEPT1) along with weaker barrier function than Caco-2 cells, thus revealing a physiologically relevant phenotype.

Besides the directed differentiation of iPSCs to specific intestinal cell types, multicellular intestinal tissues have also been developed using organoid culture technology. Sequential treatment of iPSCs with Activin A and a growth factor cocktail (FGF4 and Wnt3A, at high concentration) generated 3D spheroids containing CDX2+ hindgut-like cells (HLCs) [122]. The study revealed that individually neither FGF4 nor Wnt3A could cause DELCs to HLCs differentiation. Also, the time of exposure and the growth factor concentration affected the stable expression of CDX2. Further, these HLC spheroids were transferred to Matrigel and cultured for long-term in medium containing another cocktail (EGF, Noggin, and R-spondin-1) to direct differentiation into small intestinal organoids (SIOs). The developed SIOs contained functional enterocytes, goblet, Paneth, and enteroendocrine cells. In a different study, a distinct population of SIOs and colonic organoids (COs) were generated [123]. The authors employed specific treatment of Activin A, FGF4, and CHIR99021 to develop CDX2+ HLC spheroids. The spheroids were encapsulated in Matrigel and exposed to either SIO (containing EGF, Noggin) or COs (containing EGF, bone morphogenetic proteins (BMP)) differentiation medium. The resultant SIOs and COs exhibited differential phenotype, similar to the native tissues. The study revealed the regulatory role of BMP signaling in stable expression of special AT-rich sequence-binding protein 2 (SATB2, a definitive marker of the presumptive large intestinal epithelium) and activation posterior homeobox (HOX) genes to direct the differentiation of iPSC-derived HLC spheroids to COs.

Human intestinal organoids were generated from iPSCs following a multistep protocol involving differentiation into DELCs (Activin A, Wnt3A), HLCs (FGF4, CHIR99021), and SIOs (EGF, Noggin, CHIR99021) [124]. The differentiated cells from the organoids were cultured in a microfluidic platform with continuous media perfusion. The study revealed that the presence of physiologically relevant shear stress resulted in intestinal morphogenesis, and showed the presence of Paneth, goblet, enterocytes, enteroendocrine cells as well as LGR5+ stem cell and WD Repeat Domain 43 (WDR43)+ transit-amplifying cell population. Moreover, the developed intestine-on-chip model showed responsiveness toward exogenous stimuli (IFN-γ and TNF-α), with in vivo–like patterns.

Specific merit of iPSCs is that they also offer an endless opportunity to recapitulate patient-specific pathobiological

Table 3 Additional studies demonstrating generation of intestinal cells from human iPSCs

S. no.	Growth factors/small molecules for differentiation induction into						Research highlights	References
	DELCs	IPLCs	ELCs	HLCs	SIOs	COs		
1	Activin A, BMP4, VEGF, FGF2	FGF2	EGF, forskolin, PD98059, 5-aza, A-83-01	–	–	–	The resultant cells exhibited SI epithelial cells (SIECs)-like functions and expression profile. Differentiated cells predicted drug permeability, better than Caco-2 cells. The authors upbeat high differentiation potential of the reported methods	[127]
2	Wnt3A, Activin A	LY2090314	Wnt3A, R-spondin3, Noggin, SB202190, Dex, EGF, IGF-1	–	–	–	The study screened different growth factors and small molecules for their effectiveness in differentiating iPSCs to IPLCs and ELCs. The differentiated cells exhibited functions similar to SIECs; with a low expression of colonic epithelial cell (CECs) markers	[128]
3	Activin A	–	–	CHIR99021, FGF4	R-spondin1, Noggin, EGF, A-83-01, PD98059, 5-aza, DAPT	–	SI-like function and gene expression profiles were observed. Organoids showed the presence of different intestinal cells (enterocytes, ISCs, goblet, enteroendocrine, Paneth, smooth muscle cells, and fibroblasts)	[129]

Table 3 (continued)

S. no.	Growth factors/small molecules for differentiation induction into						Research highlights	References
	DELCs	IPLCs	ELCs	HLCs	SIOs	COs		
4	CHIR99021	–	–	CHIR99021, FGF4, Noggin	Noggin, R-spondin, EGF, MMP-8 inhibitor	–	Direct on-chip differentiation of iPSCs was done in a step-by-step manner. The developed intestinal tubules expressed markers for enterocytes, Paneth, and neuroendocrine cells. They also developed barrier function and showed responsiveness toward pro-inflammatory cytokines	[130]
5	Activin A, CHIR99021	–	–	Activin A, CHIR99021, FGF4	R-spondin1, Noggin, EGF	–	Developed organoids expressed markers of ISC, enterocytes, goblet, and Paneth cells. Retinoic acid treatment for 48 h, promoted iPSC differentiation to intestinal organoids	[131]
6	Activin A	–	–	CHIR99021, FGF4	EGF	–	Differentiated hindgut cells were cocultured with iPSC-derived vagal neural crest cells in Matrigel, to form intestinal organoids with the enteric nervous system	[132]
7	Activin A	–	–	FGF4, Wnt3A	R-spondin1, Noggin, EGF	–	The developed organoids expressed markers of enterocytes, goblet, and Paneth cells. Mesenchymal cell marker expression was also observed. Organoids were maintained for long-term and exhibited drug-metabolizing enzyme activity	[133]

Table 3 (continued)

S. no.	Growth factors/small molecules for differentiation induction into						Research highlights	References
	DELCs	IPLCs	ELCs	HLCs	SIOs	COs		
8	Activin A, Wnt3A, FGF2	–	–	FGF4, Wnt3A	R-spondin1, Noggin, EGF	–	The developed organoids expressed markers of enterocytes, goblet cells, enteroendocrine, Paneth, and proliferative cells	[134]
9	Activin A, CHIR99021	–	–	FGF4, CHIR99021	-	EGF, CHIR99021, LDN193189	Developed COs showed phenotypic characteristics, specific to the adult human colon, respectively. COs were employed for modeling colorectal cancers and drug screening	[135]
10	Activin A, BMP4, FGF2, LYS294002, CHIR99021	–	–	Activin A, FGF2, CHIR99021, retinoic acid	R-spondin1, Noggin, EGF, CHIR99021, Y-27632, prostaglandin E_2	–	The developed organoids expressed markers of enterocytes, goblet, enteroendocrine, and Paneth cells. Organoids showed responsiveness toward *Salmonella enterica* serovar Typhimurium by expressing genes associated with infection and inflammation	[136]

Dex Dexamethasone, *VEGF* vascular endothelial growth factor, *SIECs* SI epithelial cells, *IGF-1* insulin-like growth factor 1, *CECs* colonic epithelial cell, *MMP-8* matrix metalloproteinase-8

conditions in vitro. For instance, iPSCs from patients with cystic fibrosis (p.F508del mutant) were corrected using transcription activator-like effector nuclease (TALEN)-mediated repair and further employed for generating intestinal organoids [125]. Differentiation protocol employed Activin A and Wnt3A for definite endoderm (DE) specification, Wnt3A and CHIR99021 for hindgut specification, and R-spondin1, Noggin, EGF, and Wnt3A for intestinal maturation (post-embedding in Matrigel). Organoids (both corrected and non-corrected), developed using this protocol, were able to grow without a need of mesenchymal niche, which is often present in iPSC-derived organoid culture, thus, facilitating their use in a forskolin-induced swelling assay. Moreover, the organoids from corrected iPSCs showed expression of cystic fibrosis transmembrane conductance regulator (CFTR) and functional recovery of its activity, as compared to non-corrected ones. In a separate study, patient-specific SIOs and COs were generated by differentiation of iPSCs, derived from healthy and inflammatory bowel disease (IBD) patients (adult-onset and very early onset IBD) [126]. The developed organoids were used for in vitro assessment of pro-inflammatory cytokine-induced alterations in the barrier functions of healthy and diseased patients.

Additional studies in this domain are summarized in Table 3.

Conclusion and outlook

The present article depicts superiority of the intestinal tissue models with biomimetic 3D architecture (crypt-villus or crypt-lumen) over the conventional 2D models; in reflecting native-like apicobasolateral cell polarity, functional phenotype (xenobiotic metabolism and TEER values), and cellular compartmentalization (differentiated cells at the villus/luminal end, while less differentiated/stem cell niches in the crypts). However, the future of these patterned intestinal models lies in integrating native-like biochemical cues (such as matrix composition and biochemical gradients), biophysical cues (such as matrix stiffness), mechanobiological aspects (such as shear stress and peristaltic motion), and opting for suitable coculture strategies.

In this regard, microfabrication methodologies (like photolithography and laser ablation) have a limited scope of development as they are majorly employed for creating the primary molds to mirror the 3D intestinal pattern in the bulk hydrogels. Apart from primary mold fabrication, control over the distribution of biochemical and biophysical cues as well as cellular components is quite challenging. Interestingly, 3D printing could prove to be quite handy and advantageous in this context. The recent developments in tissue engineering and regenerative medicines have already validated that 3D bioprinting provides better spatiotemporal control over the distribution of different cues and cellular components [59, 137, 138]. 3D printing strategy is still in its infancy for the development of 3D intestinal models; in fact, to date, only SLA [58] and VMEPS (a type of extrusion-based 3D printing) [61] have only been employed. However, exploring newer modalities such as scaffold-free bioprinting [139], freeform bioprinting in suspension bath [140], digital light processing (DLP)-based bioprinting (an advanced version of SLA) [141], aspiration-assisted bioprinting [142], and 4D bioprinting [143] could further widen our horizon and ensure a promising future ahead.

Besides, innovative strategies for integrating native-like fluid flow and peristalsis with these 3D patterned models are also needed. Bioreactor [55] and microfluidic [72] technologies have already been explored to address these avenues; however, they still exhibit limited clinical applicability. Notably, working with hydrogel-based 3D tissue constructs is challenging as they are fragile and often undergo disintegration under continuous mechanical stress. A critical consideration should also be paid to the biodegradation susceptibility of these hydrogel-based platforms. Improving the mechanical properties of the hydrogel system (via crosslinking) is a potent strategy, but the impact of these biomechanical cues on intestinal cell behavior should be examined as well. Moreover, current research in this domain is mostly limited to use of either human cancer cell lines or intestinal crypts (derived from rats or mouse), which cannot accurately predict drug pharmacokinetics that occur in the human system. Owing to the source and ethical limitations associated with human ISCs, the use of patient-derived iPSCs, instead, may add precision to these studies. Besides, developing strategies for high-throughput platforms with multifaceted applicability is also needed and demands profound investigation.

On a concluding note, we upbeat that endeavors guided toward integrating biomimetic architectural cues with the necessary biophysicochemical and mechanical cues along with the aspects of stem cell engineering would accord for more physiologically relevant intestinal model and could further open up new vistas in the domain of personalized medicine in the near future. Breakthrough in this field could be witnessed at faster rates via dedicated collaborative efforts from engineers, material scientists, biologists, and clinicians. Policymakers and stakeholders are also an essential part of this collaborative network.

Acknowledgements TA would like to acknowledge the INSPIRE scheme, Department of Science and Technology, Government of India, for providing the fellowship.

Author contributions TA was involved in conceptualization, writing–original draft, writing–reviewing and editing; VO was involved in writing–original draft; LL was involved in writing–original draft; AA was involved in writing–original draft; TKM was involved in conceptualization, writing–reviewing and editing; PM was involved in writing–reviewing and editing; MV was involved in writing–reviewing and editing; GY was involved in writing–reviewing and editing.

Compliance with ethical standards

Conflict of interest The authors declare that they have no conflict of interest.

Ethical approval This article does not contain any studies with human or animal subjects performed by any of the authors.

References

1. Dutton JS, Hinman SS, Kim R, Wang Y, Allbritton NL (2019) Primary cell-derived intestinal models: recapitulating physiology. Trends Biotechnol 37:744–760. https://doi.org/10.1016/j.tibtech.2018.12.001
2. Volk N, Lacy B (2017) Anatomy and physiology of the small bowel. Gastrointest Endosc Clin N Am 27:1–13. https://doi.org/10.1016/j.giec.2016.08.001
3. Campbell J, Berry J, Liang Y (2019) Anatomy and physiology of the small intestine. In: Shackelford's surgery of the alimentary tract (8th edn), vol 1, Elsevier, pp 817–841. https://doi.org/10.1016/B978-0-323-40232-3.00071-6
4. Shroyer NF, Kocoshis SA (2011) Anatomy and physiology of the small and large intestines. In: Pediatric gastrointestinal and liver disease. Elsevier, pp 324–336.e2. https://doi.org/10.1016/B978-1-4377-0774-8.10031-4
5. Turner JR (2009) Intestinal mucosal barrier function in health and disease. Nat Rev Immunol 9:799–809. https://doi.org/10.1038/nri2653
6. Allaire JM, Crowley SM, Law HT, Chang S-Y, Ko H-J, Vallance BA (2018) The intestinal epithelium: central coordinator of mucosal immunity. Trends Immunol 39:677–696. https://doi.org/10.1016/j.it.2018.04.002
7. Ting H-A, von Moltke J (2019) The immune function of tuft cells at gut mucosal surfaces and beyond. J Immunol 202:1321–1329. https://doi.org/10.4049/jimmunol.1801069
8. Jiminez JA, Uwiera TC, Douglas Inglis G, Uwiera RRE (2015) Animal models to study acute and chronic intestinal inflammation in mammals. Gut Pathog 7:29. https://doi.org/10.1186/s13099-015-0076-y
9. Williams CF, Walton GE, Jiang L, Plummer S, Garaiova I, Gibson GR (2015) Comparative analysis of intestinal tract models. Annu Rev Food Sci Technol 6:329–350. https://doi.org/10.1146/annurev-food-022814-015429
10. Kararli TT (1995) Comparison of the gastrointestinal anatomy, physiology, and biochemistry of humans and commonly used laboratory animals. Biopharm Drug Dispos 16:351–380. https://doi.org/10.1002/bdd.2510160502
11. Costa J, Ahluwalia A (2019) Advances and current challenges in intestinal in vitro model engineering: a digest. Front Bioeng Biotechnol 7:144. https://doi.org/10.3389/fbioe.2019.00144
12. Liu Y, Chen Y-G (2018) 2D- and 3D-based intestinal stem cell cultures for personalized medicine. Cells 7:225. https://doi.org/10.3390/cells7120225
13. Kim HJ, Huh D, Hamilton G, Ingber DE (2012) Human gut-on-a-chip inhabited by microbial flora that experiences intestinal peristalsis-like motions and flow. Lab Chip 12:2165. https://doi.org/10.1039/c2lc40074j
14. Shin W, Hinojosa CD, Ingber DE, Kim HJ (2019) Human intestinal morphogenesis controlled by transepithelial morphogen gradient and flow-dependent physical cues in a microengineered gut-on-a-chip. iScience 15:391–406. https://doi.org/10.1016/j.isci.2019.04.037
15. Ji Y, Zhou J, Sun T, Tang K, Xiong Z, Ren Z, Yao S, Chen K, Yang F, Zhu F, Guo X (2018) Diverse preparation methods for small intestinal submucosa (SIS): decellularization, components, and structure. J Biomed Mater Res Part A 107A: 689–697. https://doi.org/10.1002/jbm.a.36582
16. Rashtbar M, Hadjati J, Ai J, Jahanzad I, Azami M, Shirian S, Ebrahimi-Barough S, Sadroddiny E (2018) Characterization of decellularized ovine small intestine submucosal layer as extracellular matrix-based scaffold for tissue engineering. J Biomed Mater Res—Part B Appl Biomater 106B: 933–944. https://doi.org/10.1002/jbm.b.33899
17. Liao J, Xu B, Zhang R, Fan Y, Xie H, Li X (2020) Applications of decellularized materials in tissue engineering: advantages, drawbacks and current improvements, and future perspectives. J Mater Chem B 8:10023–10049. https://doi.org/10.1039/D0TB01534B
18. Zhao P, Li X, Fang Q, Wang F, Ao Q, Wang X, Tian X, Tong H, Bai S, Fan J (2020) Surface modification of small intestine submucosa in tissue engineering. Regen Biomater 7:339–348. https://doi.org/10.1093/rb/rbaa014
19. Hewes SA, Wilson RL, Estes MK, Shroyer NF, Blutt SE, Grande-Allen KJ (2020) In Vitro models of the small intestine: engineering challenges and engineering solutions. Tissue Eng Part B Rev 26:313–326. https://doi.org/10.1089/ten.teb.2019.0334
20. Kim R, Wang Y, Hwang S-HJ, Attayek PJ, Smiddy NM, Reed MI, Sims CE, Allbritton NL (2018) Formation of arrays of planar, murine, intestinal crypts possessing a stem/proliferative cell compartment and differentiated cell zone. Lab Chip 18:2202–2213. https://doi.org/10.1039/C8LC00332G
21. Ladd MR, Costello CM, Gosztyla C, Werts AD, Johnson B, Fulton WB, Martin LY, Redfield EJ, Crawford B, Panaparambil R, Sodhi CP, March JC, Hackam DJ (2019) Development of intestinal scaffolds that mimic native mammalian intestinal tissue. Tissue Eng Part A 25:1225–1241. https://doi.org/10.1089/ten.tea.2018.0239
22. Chen Y, Lin Y, Davis KM, Wang Q, Rnjak-Kovacina J, Li C, Isberg RR, Kumamoto CA, Mecsas J, Kaplan DL (2015) Robust bioengineered 3D functional human intestinal epithelium. Sci Rep 5:13708. https://doi.org/10.1038/srep13708
23. Pawlina W, Ross MH (2018) Histology: a text and atlas: with correlated cell and molecular biology. Lippincott Williams & Wilkins, Philadelphia
24. Gehart H, Clevers H (2019) Tales from the crypt: new insights into intestinal stem cells. Nat Rev Gastroenterol Hepatol 16:19–34. https://doi.org/10.1038/s41575-018-0081-y
25. Qi D, Shi W, Black AR, Kuss MA, Pang X, He Y, Liu B, Duan B (2020) Repair and regeneration of small intestine: a review of current engineering approaches. Biomaterials 240:119832. https://doi.org/10.1016/j.biomaterials.2020.119832
26. Santos AJM, Lo Y-H, Mah AT, Kuo CJ (2018) The intestinal stem cell niche: homeostasis and adaptations. Trends Cell Biol 28:1062–1078. https://doi.org/10.1016/j.tcb.2018.08.001
27. Carulli AJ, Samuelson LC, Schnell S (2014) Unraveling intestinal stem cell behavior with models of crypt dynamics. Integr Biol 6:243. https://doi.org/10.1039/c3ib40163d

28. Umar S (2010) Intestinal stem cells. Curr Gastroenterol Rep 12:340–348. https://doi.org/10.1007/s11894-010-0130-3
29. Montgomery RK, Breault DT (2008) Small intestinal stem cell markers. J Anat 213:52–58. https://doi.org/10.1111/j.1469-7580.2008.00925.x
30. Smith NR, Gallagher AC, Wong MH (2016) Defining a stem cell hierarchy in the intestine: markers, caveats and controversies. J Physiol 594:4781–4790. https://doi.org/10.1113/JP271651
31. Roth S, Franken P, Sacchetti A, Kremer A, Anderson K, Sansom O, Fodde R (2012) Paneth cells in intestinal homeostasis and tissue injury. PLoS ONE 7:e38965. https://doi.org/10.1371/journal.pone.0038965
32. Hooper LV (2015) Epithelial cell contributions to intestinal immunity. In: Advances in immunology. Elsevier, vol 126, pp 129–172. https://doi.org/10.1016/bs.ai.2014.11.003
33. Banerjee A, McKinley ET, von Moltke J, Coffey RJ, Lau KS (2018) Interpreting heterogeneity in intestinal tuft cell structure and function. J Clin Invest 128:1711–1719. https://doi.org/10.1172/JCI120330
34. Mace OJ, Tehan B, Marshall F (2015) Pharmacology and physiology of gastrointestinal enteroendocrine cells. Pharmacol Res Perspect 3:e00155. https://doi.org/10.1002/prp2.155
35. Worthington JJ, Reimann F, Gribble FM (2018) Enteroendocrine cells-sensory sentinels of the intestinal environment and orchestrators of mucosal immunity. Mucosal Immunol 11:3–20. https://doi.org/10.1038/mi.2017.73
36. Gribble FM, Reimann F, Roberts GP (2018) Gastrointestinal Hormones. In: Physiology of the gastrointestinal tract (6th edn.). Elsevier, pp 31–70. https://doi.org/10.1016/B978-0-12-809954-4.00002-5
37. Birchenough GMH, Johansson MEV, Gustafsson JK, Bergström JH, Hansson GC (2015) New developments in goblet cell mucus secretion and function. Mucosal Immunol 8:712–719. https://doi.org/10.1038/mi.2015.32
38. Kim YS, Ho SB (2010) Intestinal goblet cells and mucins in health and disease: recent insights and progress. Curr Gastroenterol Rep 12:319–330. https://doi.org/10.1007/s11894-010-0131-2
39. Snoeck V, Goddeeris B, Cox E (2005) The role of enterocytes in the intestinal barrier function and antigen uptake. Microbes Infect 7:997–1004. https://doi.org/10.1016/j.micinf.2005.04.003
40. Chougule P, Herlenius G, Hernandez NM, Patil PB, Xu B, Sumitran-Holgersson S (2012) Isolation and characterization of human primary enterocytes from small intestine using a novel method. Scand J Gastroenterol 47:1334–1343. https://doi.org/10.3109/00365521.2012.708940
41. Gonzalez LM, Williamson I, Piedrahita JA, Blikslager AT, Magness ST (2013) Cell lineage identification and stem cell culture in a porcine model for the study of intestinal epithelial regeneration. PLoS ONE 8:e66465. https://doi.org/10.1371/journal.pone.0066465
42. Ohno H (2016) Intestinal M cells. J Biochem 159:151–160. https://doi.org/10.1093/jb/mvv121
43. Mabbott NA, Donaldson DS, Ohno H, Williams IR, Mahajan A (2013) Microfold (M) cells: important immunosurveillance posts in the intestinal epithelium. Mucosal Immunol 6:666–677. https://doi.org/10.1038/mi.2013.30
44. Paik S, Kim G, Chang S, Lee S, Jin D, Jeong K-Y, Lee IS, Lee J, Moon H, Lee J, Chang K, Choi SS, Moon J, Jung S, Kang S, Lee W, Choi H-J, Choi H, Kim HJ, Lee J-H, Cheon J, Kim M, Myoung J, Park H-G, Shim W (2020) Near-field sub-diffraction photolithography with an elastomeric photomask. Nat Commun 11:805. https://doi.org/10.1038/s41467-020-14439-1
45. Cho CH, Kwon S, Park J-K (2017) Assembly of hydrogel units for 3D microenvironment in a poly(dimethylsiloxane) channel. Micro Nano Syst Lett 5:2. https://doi.org/10.1186/s40486-016-0035-5
46. Wang Y, Kim R, Gunasekara DB, Reed MI, DiSalvo M, Nguyen DL, Bultman SJ, Sims CE, Magness ST, Allbritton NL (2018) Formation of human colonic crypt array by application of chemical gradients across a shaped epithelial monolayer. Cell Mol Gastroenterol Hepatol 5:113–130. https://doi.org/10.1016/j.jcmgh.2017.10.007
47. Hinman SS, Wang Y, Allbritton NL (2019) Photopatterned membranes and chemical gradients enable scalable phenotypic organization of primary human colon epithelial models. Anal Chem 91:15240–15247. https://doi.org/10.1021/acs.analchem.9b04217
48. Wang Y, Gunasekara DB, Reed MI, DiSalvo M, Bultman SJ, Sims CE, Magness ST, Allbritton NL (2017) A microengineered collagen scaffold for generating a polarized crypt-villus architecture of human small intestinal epithelium. Biomaterials 128:44–55. https://doi.org/10.1016/j.biomaterials.2017.03.005
49. Castaño AG, García-Díaz M, Torras N, Altay G, Comelles J, Martínez E (2019) Dynamic photopolymerization produces complex microstructures on hydrogels in a moldless approach to generate a 3D intestinal tissue model. Biofabrication 11:025007. https://doi.org/10.1088/1758-5090/ab0478
50. Yang W-C, Chen Y-C, Huang Y-S, Fu Y-Y, Tang S-C, Fu C-C (2012) Engineering a biomimetic villus array for in vitro three-dimensional culture of intestinal epithelial cells. J Microelectromech Syst 21:1418–1425. https://doi.org/10.1109/JMEMS.2012.2205902
51. Sung JH, Yu J, Luo D, Shuler ML, March JC (2011) Microscale 3-D hydrogel scaffold for biomimetic gastrointestinal (GI) tract model. Lab Chip 11:389–392. https://doi.org/10.1039/C0LC00273A
52. Kim SH, Chi M, Yi B, Kim SH, Oh S, Kim Y, Park S, Sung JH (2014) Three-dimensional intestinal villi epithelium enhances protection of human intestinal cells from bacterial infection by inducing mucin expression. Integr Biol 6:1122–1131. https://doi.org/10.1039/c4ib00157e
53. Yu J, Peng S, Luo D, March JC (2012) In vitro 3D human small intestinal villous model for drug permeability determination. Biotechnol Bioeng 109:2173–2178. https://doi.org/10.1002/bit.24518
54. Costello CM, Hongpeng J, Shaffiey S, Yu J, Jain NK, Hackam D, March JC (2014) Synthetic small intestinal scaffolds for improved studies of intestinal differentiation. Biotechnol Bioeng 111:1222–1232. https://doi.org/10.1002/bit.25180
55. Costello CM, Phillipsen MB, Hartmanis LM, Kwasnica MA, Chen V, Hackam D, Chang MW, Bentley WE, March JC (2017) Microscale Bioreactors for in situ characterization of GI epithelial cell physiology. Sci Rep 7:12515. https://doi.org/10.1038/s41598-017-12984-2
56. Koppes AN, Kamath M, Pfluger CA, Burkey DD, Dokmeci M, Wang L, Carrier RL (2016) Complex, multi-scale small intestinal topography replicated in cellular growth substrates fabricated via chemical vapor deposition of Parylene C. Biofabrication 8:035011. https://doi.org/10.1088/1758-5090/8/3/035011
57. Capel AJ, Rimington RP, Lewis MP, Christie SDR (2018) 3D printing for chemical, pharmaceutical and biological applications. Nat Rev Chem 2:422–436. https://doi.org/10.1038/s41570-018-0058-y
58. Creff J, Courson R, Mangeat T, Foncy J, Souleille S, Thibault C, Besson A, Malaquin L (2019) Fabrication of 3D scaffolds reproducing intestinal epithelium topography by high-resolution 3D stereolithography. Biomaterials 221:119404. https://doi.org/10.1016/j.biomaterials.2019.119404
59. Murphy SV, Atala A (2014) 3D bioprinting of tissues and organs. Nat Biotechnol 32:773–785. https://doi.org/10.1038/nbt.2958

60. Truby RL, Lewis JA (2016) Printing soft matter in three dimensions. Nature 540:371–378. https://doi.org/10.1038/nature21003
61. Kim W, Kim GH (2018) An innovative cell-printed microscale collagen model for mimicking intestinal villus epithelium. Chem Eng J 334:2308–2318. https://doi.org/10.1016/j.cej.2017.12.001
62. Kim W, Kim G (2018) Intestinal villi model with blood capillaries fabricated using collagen-based bioink and dual-cell-printing process. ACS Appl Mater Interfaces 10:41185–41196. https://doi.org/10.1021/acsami.8b17410
63. Kim W, Kim GH (2020) An intestinal model with a finger-like villus structure fabricated using a bioprinting process and collagen/SIS-based cell-laden bioink. Theranostics 10:2495–2508. https://doi.org/10.7150/thno.41225
64. Huang J, Chen Y, Tang C, Fei Y, Wu H, Ruan D, Paul ME, Chen X, Yin Z, Heng BC, Chen W, Shen W (2019) The relationship between substrate topography and stem cell differentiation in the musculoskeletal system. Cell Mol Life Sci 76:505–521. https://doi.org/10.1007/s00018-018-2945-2
65. Agarwal T, Subramanian B, Maiti TK (2019) Liver tissue engineering: challenges and opportunities. ACS Biomater Sci Eng 5:4167–4182. https://doi.org/10.1021/acsbiomaterials.9b00745
66. Karbassi E, Fenix A, Marchiano S, Muraoka N, Nakamura K, Yang X, Murry CE (2020) Cardiomyocyte maturation: advances in knowledge and implications for regenerative medicine. Nat Rev Cardiol 17:341–359. https://doi.org/10.1038/s41569-019-0331-x
67. Yi B, Shim KY, Ha SK, Han J, Hoang H-H, Choi I, Park S, Sung JH (2017) Three-dimensional in vitro gut model on a villi-shaped collagen scaffold. BioChip J 11:219–231. https://doi.org/10.1007/s13206-017-1307-8
68. Gommers LMM, Skrzypek K, Bolhuis-Versteeg L, Pinckaers NET, Vrijhof R, van der Wijst J, de Baaij JHF, Stamatialis D, Hoenderop JGJ (2019) Development of a villi-like micropatterned porous membrane for intestinal magnesium and calcium uptake studies. Acta Biomater 99:110–120. https://doi.org/10.1016/j.actbio.2019.08.041
69. Clevers H (2013) The intestinal crypt, a prototype stem cell compartment. Cell 154:274–284. https://doi.org/10.1016/j.cell.2013.07.004
70. Wang Y, Gunasekara DB, Attayek PJ, Reed MI, DiSalvo M, Nguyen DL, Dutton JS, Lebhar MS, Bultman SJ, Sims CE, Magness ST, Allbritton NL (2017) In vitro generation of mouse colon crypts. ACS Biomater Sci Eng 3:2502–2513. https://doi.org/10.1021/acsbiomaterials.7b00368
71. Esch MB, Sung JH, Yang J, Yu C, Yu J, March JC, Shuler ML (2012) On chip porous polymer membranes for integration of gastrointestinal tract epithelium with microfluidic 'body-on-a-chip' devices. Biomed Microdevices 14:895–906. https://doi.org/10.1007/s10544-012-9669-0
72. Shim K-Y, Lee D, Han J, Nguyen N-T, Park S, Sung JH (2017) Microfluidic gut-on-a-chip with three-dimensional villi structure. Biomed Microdevices 19:37. https://doi.org/10.1007/s10544-017-0179-y
73. Elomaa L, Keshi E, Sauer IM, Weinhart M (2020) Development of GelMA/PCL and dECM/PCL resins for 3D printing of acellular in vitro tissue scaffolds by stereolithography. Mater Sci Eng C 112:110958. https://doi.org/10.1016/j.msec.2020.110958
74. Lee M, Dunn JCY, Wu BM (2005) Scaffold fabrication by indirect three-dimensional printing. Biomaterials 26:4281–4289. https://doi.org/10.1016/j.biomaterials.2004.10.040
75. Costello CM, Sorna RM, Goh Y-L, Cengic I, Jain NK, March JC (2014) 3-D intestinal scaffolds for evaluating the therapeutic potential of probiotics. Mol Pharm 11:2030–2039. https://doi.org/10.1021/mp5001422
76. Hubbell JA (2014) Matrix efects. In: Principles of tissue engineering. Elsevier, pp 407–421. https://doi.org/10.1016/B978-0-12-398358-9.00021-5
77. Frantz C, Stewart KM, Weaver VM (2010) The extracellular matrix at a glance. J Cell Sci 123:4195–4200. https://doi.org/10.1242/jcs.023820
78. Kim TG, Shin H, Lim DW (2012) Biomimetic scaffolds for tissue engineering. Adv Funct Mater 22:2446–2468. https://doi.org/10.1002/adfm.201103083
79. Godfrey M (2009) Extracellular Matrix. In: Asthma and COPD. Elsevier, pp 265–274. https://doi.org/10.1016/B978-0-12-374001-4.00022-5
80. Muncie JM, Weaver VM (2018) Chapter one—the physical and biochemical properties of the extracellular matrix regulate cell fate. In: Litscher ES, Wassarman PMBT-CT in DB (eds) Extracellular matrix and egg coats. Academic Press, New York, pp 1–37
81. Wang Y, Kim R, Hinman SS, Zwarycz B, Magness ST, Allbritton NL (2018) Bioengineered systems and designer matrices that recapitulate the intestinal stem cell niche. Cell Mol Gastroenterol Hepatol 5:440-453.e1. https://doi.org/10.1016/j.jcmgh.2018.01.008
82. Teller IC, Beaulieu J-F (2001) Interactions between laminin and epithelial cells in intestinal health and disease. Expert Rev Mol Med 3:1–18. https://doi.org/10.1017/S1462399401003623
83. Beaulieu JF (1992) Differential expression of the VLA family of integrins along the crypt-villus axis in the human small intestine. J Cell Sci 102:427–436
84. Meran L, Baulies A, Li VSW (2017) Intestinal stem cell niche: the extracellular matrix and cellular components. Stem Cells Int 2017:1–11. https://doi.org/10.1155/2017/7970385
85. Yamamoto S, Nakase H, Matsuura M, Honzawa Y, Matsumura K, Uza N, Yamaguchi Y, Mizoguchi E, Chiba T (2013) Heparan sulfate on intestinal epithelial cells plays a critical role in intestinal crypt homeostasis via Wnt/β-catenin signaling. Am J Physiol Liver Physiol 305:G241–G249. https://doi.org/10.1152/ajpgi.00480.2012
86. Tong Z, Martyn K, Yang A, Yin X, Mead BE, Joshi N, Sherman NE, Langer RS, Karp JM (2018) Towards a defined ECM and small molecule based monolayer culture system for the expansion of mouse and human intestinal stem cells. Biomaterials 154:60–73. https://doi.org/10.1016/j.biomaterials.2017.10.038
87. Hernandez-Gordillo V, Kassis T, Lampejo A, Choi G, Gamboa ME, Gnecco JS, Breault DT, Carrier R, Griffith LG (2019) Niche-inspired synthetic matrices for epithelial organoid culture. bioRxiv. https://doi.org/10.1101/806919
88. Gjorevski N, Sachs N, Manfrin A, Giger S, Bragina ME, Ordóñez-Morán P, Clevers H, Lutolf MP (2016) Designer matrices for intestinal stem cell and organoid culture. Nature 539:560–564. https://doi.org/10.1038/nature20168
89. Broguiere N, Isenmann L, Hirt C, Ringel T, Placzek S, Cavalli E, Ringnalda F, Villiger L, Züllig R, Lehmann R, Rogler G, Heim MH, Schüler J, Zenobi-Wong M, Schwank G (2018) Growth of epithelial organoids in a defined hydrogel. Adv Mater 30:1801621. https://doi.org/10.1002/adma.201801621
90. DiMarco RL, Dewi RE, Bernal G, Kuo C, Heilshorn SC (2015) Protein-engineered scaffolds for in vitro 3D culture of primary adult intestinal organoids. Biomater Sci 3:1376–1385. https://doi.org/10.1039/C5BM00108K
91. DiMarco RL, Hunt DR, Dewi RE, Heilshorn SC (2017) Improvement of paracellular transport in the Caco-2 drug screening model using protein-engineered substrates. Biomaterials 129:152–162. https://doi.org/10.1016/j.biomaterials.2017.03.023
92. Wang L, Murthy SK, Barabino GA, Carrier RL (2010) Synergic effects of crypt-like topography and ECM proteins on intestinal cell behavior in collagen based membranes.

Biomaterials 31:7586–7598. https://doi.org/10.1016/j.biomaterials.2010.06.036
93. Hadden WJ, Young JL, Holle AW, McFetridge ML, Kim DY, Wijesinghe P, Taylor-Weiner H, Wen JH, Lee AR, Bieback K, Vo B-N, Sampson DD, Kennedy BF, Spatz JP, Engler AJ, Choi YS (2017) Stem cell migration and mechanotransduction on linear stiffness gradient hydrogels. Proc Natl Acad Sci 114:5647–5652. https://doi.org/10.1073/pnas.1618239114
94. Xia T, Liu W, Yang L (2017) A review of gradient stiffness hydrogels used in tissue engineering and regenerative medicine. J Biomed Mater Res Part A 105:1799–1812. https://doi.org/10.1002/jbm.a.36034
95. Altay G, Larrañaga E, Tosi S, Barriga FM, Batlle E, Fernández-Majada V, Martínez E (2019) Self-organized intestinal epithelial monolayers in crypt and villus-like domains show effective barrier function. Sci Rep 9:10140. https://doi.org/10.1038/s41598-019-46497-x
96. Speer JE, Gunasekara DB, Wang Y, Fallon JK, Attayek PJ, Smith PC, Sims CE, Allbritton NL (2019) Molecular transport through primary human small intestinal monolayers by culture on a collagen scaffold with a gradient of chemical cross-linking. J Biol Eng 13:36. https://doi.org/10.1186/s13036-019-0165-4
97. Speer JE, Wang Y, Fallon JK, Smith PC, Allbritton NL (2019) Evaluation of human primary intestinal monolayers for drug metabolizing capabilities. J Biol Eng 13:82. https://doi.org/10.1186/s13036-019-0212-1
98. Kim HJ, Ingber DE (2013) Gut-on-a-Chip microenvironment induces human intestinal cells to undergo villus differentiation. Integr Biol 5:1130. https://doi.org/10.1039/c3ib40126j
99. Delon LC, Guo Z, Oszmiana A, Chien C-C, Gibson R, Prestidge C, Thierry B (2019) A systematic investigation of the effect of the fluid shear stress on Caco-2 cells towards the optimization of epithelial organ-on-chip models. Biomaterials 225:119521. https://doi.org/10.1016/j.biomaterials.2019.119521
100. Zhang J, Li W, Sanders MA, Sumpio BE, Asit P, Basson MD (2003) Regulation of the intestinal epithelial response to cyclic strain by extracellular matrix proteins. FASEB J 17:1–22. https://doi.org/10.1096/fj.02-0663fje
101. Poling HM, Wu D, Brown N, Baker M, Hausfeld TA, Huynh N, Chaffron S, Dunn JCY, Hogan SP, Wells JM, Helmrath MA, Mahe MM (2018) Mechanically induced development and maturation of human intestinal organoids in vivo. Nat Biomed Eng 2:429–442. https://doi.org/10.1038/s41551-018-0243-9
102. Lozoya-Agullo I, Araújo F, González-Álvarez I, Merino-Sanjuán M, González-Álvarez M, Bermejo M, Sarmento B (2017) Usefulness of Caco-2/HT29-MTX and Caco-2/HT29-MTX/Raji B coculture models to predict intestinal and colonic permeability compared to Caco-2 monoculture. Mol Pharm 14:1264–1270. https://doi.org/10.1021/acs.molpharmaceut.6b01165
103. Wang Q, Wang K, Solorzano-Vargas RS, Lin P-Y, Walthers CM, Thomas A-L, Martín MG, Dunn JCY (2018) Bioengineered intestinal muscularis complexes with long-term spontaneous and periodic contractions. PLoS ONE 13:e0195315. https://doi.org/10.1371/journal.pone.0195315
104. Kasendra M, Tovaglieri A, Sontheimer-Phelps A, Jalili-Firoozinezhad S, Bein A, Chalkiadaki A, Scholl W, Zhang C, Rickner H, Richmond CA, Li H, Breault DT, Ingber DE (2018) Development of a primary human small intestine-on-a-chip using biopsy-derived organoids. Sci Rep 8:2871. https://doi.org/10.1038/s41598-018-21201-7
105. Vila A, Torras N, Castaño AG, García-Díaz M, Comelles J, Pérez-Berezo T, Corregidor C, Castaño Ó, Engel E, Fernández-Majada V, Martínez E (2020) Hydrogel co-networks of gelatine methacrylate and poly(ethylene glycol) diacrylate sustain 3D functional in vitro models of intestinal mucosa. Biofabrication 12:025008. https://doi.org/10.1088/1758-5090/ab5f50
106. Zhou W, Chen Y, Roh T, Lin Y, Ling S, Zhao S, Lin JD, Khalil N, Cairns DM, Manousiouthakis E, Tse M, Kaplan DL (2018) Multifunctional bioreactor system for human intestine tissues. ACS Biomater Sci Eng 4:231–239. https://doi.org/10.1021/acsbiomaterials.7b00794
107. Lahar N, Lei NY, Wang J, Jabaji Z, Tung SC, Joshi V, Lewis M, Stelzner M, Martín MG, Dunn JCY (2011) Intestinal subepithelial myofibroblasts support in vitro and in vivo growth of human small intestinal epithelium. PLoS ONE 6:e26898. https://doi.org/10.1371/journal.pone.0026898
108. Jabaji Z, Brinkley GJ, Khalil HA, Sears CM, Lei NY, Lewis M, Stelzner M, Martín MG, Dunn JCY (2014) Type I collagen as an extracellular matrix for the in vitro growth of human small intestinal epithelium. PLoS ONE 9:e107814. https://doi.org/10.1371/journal.pone.0107814
109. Puzan M, Hosic S, Ghio C, Koppes A (2018) Enteric nervous system regulation of intestinal stem cell differentiation and epithelial monolayer function. Sci Rep 8:6313. https://doi.org/10.1038/s41598-018-24768-3
110. Min S, Kim S, Cho S-W (2020) Gastrointestinal tract modeling using organoids engineered with cellular and microbiota niches. Exp Mol Med 52:227–237. https://doi.org/10.1038/s12276-020-0386-0
111. Thursby E, Juge N (2017) Introduction to the human gut microbiota. Biochem J 474:1823–1836. https://doi.org/10.1042/BCJ20160510
112. Hou Q, Ye L, Liu H, Huang L, Yang Q, Turner J, Yu Q (2018) Lactobacillus accelerates ISCs regeneration to protect the integrity of intestinal mucosa through activation of STAT3 signaling pathway induced by LPLs secretion of IL-22. Cell Death Differ 25:1657–1670. https://doi.org/10.1038/s41418-018-0070-2
113. Kim HJ, Li H, Collins JJ, Ingber DE (2016) Contributions of microbiome and mechanical deformation to intestinal bacterial overgrowth and inflammation in a human gut-on-a-chip. Proc Natl Acad Sci 113:E7–E15. https://doi.org/10.1073/pnas.1522193112
114. Donohoe DR, Garge N, Zhang X, Sun W, O'Connell TM, Bunger MK, Bultman SJ (2011) The microbiome and butyrate regulate energy metabolism and autophagy in the mammalian colon. Cell Metab 13:517–526. https://doi.org/10.1016/j.cmet.2011.02.018
115. Kaiko GE, Ryu SH, Koues OI, Collins PL, Solnica-Krezel L, Pearce EJ, Pearce EL, Oltz EM, Stappenbeck TS (2016) The colonic crypt protects stem cells from microbiota-derived metabolites. Cell 165:1708–1720. https://doi.org/10.1016/j.cell.2016.05.018
116. Peng L, He Z, Chen W, Holzman IR, Lin J (2007) Effects of butyrate on intestinal barrier function in a Caco-2 cell monolayer model of intestinal barrier. Pediatr Res 61:37–41. https://doi.org/10.1203/01.pdr.0000250014.92242.f3
117. Matsumoto M, Kibe R, Ooga T, Aiba Y, Kurihara S, Sawaki E, Koga Y, Benno Y (2012) Impact of intestinal microbiota on intestinal luminal metabolome. Sci Rep 2:233. https://doi.org/10.1038/srep00233
118. Löser C, Eisel A, Harms D, Fölsch UR (1999) Dietary polyamines are essential luminal growth factors for small intestinal and colonic mucosal growth and development. Gut 44:12–16. https://doi.org/10.1136/gut.44.1.12
119. Iwao T, Toyota M, Miyagawa Y, Okita H, Kiyokawa N, Akutsu H, Umezawa A, Nagata K, Matsunaga T (2014) Differentiation of human induced pluripotent stem cells into functional enterocyte-like cells using a simple method. Drug Metab Pharmacokinet 29:44–51. https://doi.org/10.2133/dmpk.DMPK-13-RG-005
120. Iwao T, Kodama N, Kondo Y, Kabeya T, Nakamura K, Horikawa T, Niwa T, Kurose K, Matsunaga T (2015) Generation of enterocyte-like cells with pharmacokinetic functions from human induced pluripotent stem cells using small-molecule compounds.

Drug Metab Dispos 43:603–610. https://doi.org/10.1124/dmd.114.062604
121. Ozawa T, Takayama K, Okamoto R, Negoro R, Sakurai F, Tachibana M, Kawabata K, Mizuguchi H (2015) Generation of enterocyte-like cells from human induced pluripotent stem cells for drug absorption and metabolism studies in human small intestine. Sci Rep 5:16479. https://doi.org/10.1038/srep16479
122. Spence JR, Mayhew CN, Rankin SA, Kuhar MF, Vallance JE, Tolle K, Hoskins EE, Kalinichenko VV, Wells SI, Zorn AM, Shroyer NF, Wells JM (2011) Directed differentiation of human pluripotent stem cells into intestinal tissue in vitro. Nature 470:105–109. https://doi.org/10.1038/nature09691
123. Múnera JO, Sundaram N, Rankin SA, Hill D, Watson C, Mahe M, Vallance JE, Shroyer NF, Sinagoga KL, Zarzoso-Lacoste A, Hudson JR, Howell JC, Chatuvedi P, Spence JR, Shannon JM, Zorn AM, Helmrath MA, Wells JM (2017) Differentiation of human pluripotent stem cells into colonic organoids via transient activation of bmp signaling. Cell Stem Cell 21:51-64.e6. https://doi.org/10.1016/j.stem.2017.05.020
124. Workman MJ, Gleeson JP, Troisi EJ, Estrada HQ, Kerns SJ, Hinojosa CD, Hamilton GA, Targan SR, Svendsen CN, Barrett RJ (2018) Enhanced utilization of induced pluripotent stem cell-derived human intestinal organoids using microengineered chips. Cell Mol Gastroenterol Hepatol 5:669-677.e2. https://doi.org/10.1016/j.jcmgh.2017.12.008
125. Fleischer A, Vallejo-Díez S, Martín-Fernández JM, Sánchez-Gilabert A, Castresana M, del Pozo A, Esquisabel A, Ávila S, Castrillo JL, Gaínza E, Pedraz JL, Viñas M, Bachiller D (2020) iPSC-derived intestinal organoids from cystic fibrosis patients acquire CFTR activity upon TALEN-mediated repair of the p.F508del mutation. Mol Ther—Methods Clin Dev 17:858–870. https://doi.org/10.1016/j.omtm.2020.04.005
126. Gleeson JP, Estrada HQ, Yamashita M, Svendsen CN, Targan SR, Barrett RJ (2020) Development of physiologically responsive human ipsc-derived intestinal epithelium to study barrier dysfunction in IBD. Int J Mol Sci 21:1438. https://doi.org/10.3390/ijms21041438
127. Kabeya T, Mima S, Imakura Y, Miyashita T, Ogura I, Yamada T, Yasujima T, Yuasa H, Iwao T, Matsunaga T (2020) Pharmacokinetic functions of human induced pluripotent stem cell-derived small intestinal epithelial cells. Drug Metab Pharmacokinet 35:374–382. https://doi.org/10.1016/j.dmpk.2020.04.334
128. Negoro R, Takayama K, Kawai K, Harada K, Sakurai F, Hirata K, Mizuguchi H (2018) Efficient generation of small intestinal epithelial-like cells from human iPSCs for drug absorption and metabolism studies. Stem Cell Rep 11:1539–1550. https://doi.org/10.1016/j.stemcr.2018.10.019
129. Onozato D, Yamashita M, Nakanishi A, Akagawa T, Kida Y, Ogawa I, Hashita T, Iwao T, Matsunaga T (2018) Generation of intestinal organoids suitable for pharmacokinetic studies from human induced pluripotent stem cells. Drug Metab Dispos 46:1572–1580. https://doi.org/10.1124/dmd.118.080374
130. Naumovska E, Aalderink G, Wong Valencia C, Kosim K, Nicolas A, Brown S, Vulto P, Erdmann KS, Kurek D (2020) Direct on-chip differentiation of intestinal tubules from induced pluripotent stem cells. Int J Mol Sci 21:4964. https://doi.org/10.3390/ijms21144964
131. Yamada S, Kanda Y (2019) Retinoic acid promotes barrier functions in human iPSC-derived intestinal epithelial monolayers. J Pharmacol Sci 140:337–344. https://doi.org/10.1016/j.jphs.2019.06.012
132. Loffet E, Brossard L, Mahe MM (2020) Pluripotent stem cell derived intestinal organoids with an enteric nervous system. In: Spence JRBT-M in CB (ed) Human pluripotent stem cell derived organoid models. Academic Press, New York, pp 175–199
133. Yoshida S, Miwa H, Kawachi T, Kume S, Takahashi K (2020) Generation of intestinal organoids derived from human pluripotent stem cells for drug testing. Sci Rep 10:5989. https://doi.org/10.1038/s41598-020-63151-z
134. Takahashi Y, Sato S, Kurashima Y, Yamamoto T, Kurokawa S, Yuki Y, Takemura N, Uematsu S, Lai C-Y, Otsu M, Matsuno H, Osawa H, Mizushima T, Nishimura J, Hayashi M, Yamaguchi T, Kiyono H (2018) A Refined culture system for human induced pluripotent stem cell-derived intestinal epithelial organoids. Stem Cell Rep 10:314–328. https://doi.org/10.1016/j.stemcr.2017.11.004
135. Crespo M, Vilar E, Tsai S-Y, Chang K, Amin S, Srinivasan T, Zhang T, Pipalia NH, Chen HJ, Witherspoon M, Gordillo M, Xiang JZ, Maxfield FR, Lipkin S, Evans T, Chen S (2017) Colonic organoids derived from human induced pluripotent stem cells for modeling colorectal cancer and drug testing. Nat Med 23:878–884. https://doi.org/10.1038/nm.4355
136. Forbester JL, Goulding D, Vallier L, Hannan N, Hale C, Pickard D, Mukhopadhyay S, Dougan G (2015) Interaction of salmonella enterica serovar typhimurium with intestinal organoids derived from human induced pluripotent stem cells. Infect Immun 83:2926–2934. https://doi.org/10.1128/IAI.00161-15
137. Matai I, Kaur G, Seyedsalehi A, McClinton A, Laurencin CT (2020) Progress in 3D bioprinting technology for tissue/organ regenerative engineering. Biomaterials 226:119536. https://doi.org/10.1016/j.biomaterials.2019.119536
138. Mandrycky C, Wang Z, Kim K, Kim D-H (2016) 3D bioprinting for engineering complex tissues. Biotechnol Adv 34:422–434. https://doi.org/10.1016/j.biotechadv.2015.12.011
139. Murata D, Arai K, Nakayama K (2020) Scaffold-free bio-3d printing using spheroids as "bio-inks" for tissue (re-)construction and drug response tests. Adv Healthc Mater 9:1901831. https://doi.org/10.1002/adhm.201901831
140. McCormack A, Highley CB, Leslie NR, Melchels FPW (2020) 3D Printing in suspension baths: keeping the promises of bioprinting afloat. Trends Biotechnol 38:584–593. https://doi.org/10.1016/j.tibtech.2019.12.020
141. Zhang J, Hu Q, Wang S, Tao J, Gou M (2019) Digital light processing based three-dimensional printing for medical applications. Int J Bioprint 6:1. https://doi.org/10.18063/ijb.v6i1.242
142. Ayan B, Heo DN, Zhang Z, Dey M, Povilianskas A, Drapaca C, Ozbolat IT (2020) Aspiration-assisted bioprinting for precise positioning of biologics. Sci Adv 6:eaaw5111. https://doi.org/10.1126/sciadv.aaw5111
143. Gao B, Yang Q, Zhao X, Jin G, Ma Y, Xu F (2016) 4D bioprinting for biomedical applications. Trends Biotechnol 34:746–756. https://doi.org/10.1016/j.tibtech.2016.03.004